DEPARTMENT OF DEFENCE
DEFENCE SCIENCE & TECHNOLOGY ORGANISATION
DSTO

An Investigation of Target Detection Ability Using Spectral Signatures at Hyperspectral Resolution

T.P. Bubner, S.K. Kempinger and V.K. Shettigara

DSTO-TR-0807

An Investigation of Target Detection Ability Using Spectral Signatures at Hyperspectral Resolution.

T. P. Bubner, S. K. Kempinger and V. K. Shettigara.

Surveillance Systems Division
Electronics and Surveillance Research Laboratory

DSTO-TR-0807

ABSTRACT

This report addresses a variety of issues expected to influence the performance of airborne high spectral resolution (hyperspectral) Electro-Optic (EO) sensors when used as surveillance tools. Fundamental phenomenology issues have been considered with the breadth of this study ranging from investigation into the reflectance properties of materials, the influence of the atmosphere, and modelling of a sensor's performance. Simple data analysis and target detection assessment techniques including Target to Clutter Ratio measures and single and multiple band 'likelihood ratio detection' have been employed on an illustrative example. Initial results are promising, indicating high probabilities of detection with low false alarm rates for the test example.

Approved for public release

DEPARTMENT OF DEFENCE
DEFENCE SCIENCE & TECHNOLOGY ORGANISATION **DSTO**

Published by

DSTO
Electronics and Surveillance Research Laboratory
PO Box 1500
Salisbury South Australia 5108 Australia

Telephone: (08) 8259 5555
Fax: (08) 8259 6567

AR-010-899
February 2001

APPROVED FOR PUBLIC RELEASE

Authors

Tim Bubner
Surveillance Systems Division

Timothy P. Bubner is a Senior Research Scientist within DSTO. He has a PhD in Chemistry from the University of Adelaide. He has published in the area of preparative organic chemistry, and has worked in the areas of Non-Linear and laser optics, EO atmospheric propagation modelling and the spectroscopic and hyperspectral phenomenological investigations of materials.

Siegfried G. Kempinger
Surveillance Systems Division

Siegfried G. Kempinger is a Professional Officer Grade 2 within DSTO. He has an Applied Science Degree in Natural Resource Management (Ecology) from the University of Adelaide. He has previously worked as a Land Manager in the Northern Territory and as a Tutor in Remote Sensing at Adelaide University. At DSTO, his principal areas of work have been in the field of remote sensing and image processing applied to multispectral and synthetic aperture radar image data. He is currently investigating the phenomenology of sensor data at hyperspectral resolution for target detection using forward modelling and simulation techniques.

Vittala K. Shettigara
Surveillance Systems Division

Vittala K. Shettigara is a Senior Research Scientist with DSTO. He has a Ph.D in Geophysics from the University of Hawaii and his specialisation was in electrical methods of prospecting and numerical modelling. After his Ph.D. he worked as a Post-doctoral fellow with the Centre for Remote Sensing, University of New South Wales. In remote sensing he has published in the fields of pattern recognition, computer vision, change detection and image enhancement. Since 1989 Vittala has worked in DSTO in the areas of remote sensing and image processing. His current interests are in hyperspectral data processing algorithms, modelling and simulation, and in multispectral sensor capability assessment.

An Investigation of Target Detection Ability Using Spectral Signatures at Hyperspectral Resolution.

Executive Summary

This report addresses a variety of issues, which are expected to influence the performance of hyperspectral sensors as surveillance tools. Fundamental phenomenology issues have been considered and analysis and results built upon this foundation. The breadth of this study has ranged from investigation into the reflectance properties of materials, the influence of the atmosphere, a sensor's performance, data analysis and target detection assessment. Although the initial results are good, they need to be taken as indicative only, due to the limited scope of the analysis.

This study has demonstrated that a sensor operating at hyperspectral resolution has potential for detecting targets such as green camouflage in an eucalypt background with high probability and a low false alarm rate. Such targets would be expected to be difficult to detect by lower spectral resolution devices of similar spatial resolution. The ability to detect 'sub-pixel' targets is confirmed, with the case presented indicating high detection probabilities and low false alarm rates even when the target occupies only 20% of the pixel. These results are consistent with findings reported by several other researchers.

When excluding other performance limiting factors, atmosphere propagation, altitude and geometry variations were found not to markedly alter the test case's single band analysis, target and background separation, and hence detection performance. If both targets and background are influenced equally then the Target to Clutter Ratio (TCR) measure remains constant.

Under normal midday operational conditions target detection performance was not system noise limited. Only under low light or poor target and background separation conditions was system noise observed to influence detection performance appreciably.

An approach has been outlined for the assesment of target detection performance for a selected surveillance scenario. A sound procedure has been developed upon which this work can be extended to include the identification of the most appropriate spectral channels, their band-width and sampling intervals for the given surveillance scenario. This procedure also provides a platform for further studies to better quantify the performance and operational parameters of hyperspectral surveillance sensors.

Contents

1. Introduction

1.1 Background

The electro-optic (EO) spectrum from 0.4 to 15 micrometers (μm) contains a vast reservoir of information about the environment and the effects of anthropogenic activity within it. Efficient use of all this information should enhance defence capability.[1]

As EO technology has evolved, the development of tools to explore regions outside the usual visible range (0.4 to 0.7 μm) has blossomed. While there is broad scope for discussion on systems and technologies suitable for EO detection, this report is interested in investigating issues associated with the potential utility of high spectral resolution sensors as broad area surveillance tools.

Effective surveillance of the vast, sparsely populated regions of Northern Australia has been identified as being of importance in the strategic defence of Australia. This has been flagged by the JP-129 project, and significant efforts are currently under way to assess the suitability of selected tools including Synthetic Aperture Radar and EO systems to meet the project objectives.

Hyperspectral (HS) imaging presents as a technology that may be suitable to address some of the JP-129 objectives. Before this technology can be incorporated into surveillance systems, significant investigations are needed to address its potential operational effectiveness. This report is directed at investigating some of the phenomenology associated with this technology in the reflective part of the EO spectrum (0.4 to 2.5 μm) and to develop an approach to assess likely target detection performance.

HS imaging systems normally collect between 100-300 spectral bands and operate at a spectral resolution ($\Delta\lambda/\lambda$) around 0.01, where $\Delta\lambda$ represents the width of the individual spectral bands and λ the extent of the HS system's entire operational spectral range. This resolution corresponds to approximately a 10 to 20 nanometre (nm) spectral bandwidth for a 'reflective' HS sensor operating between 0.4 to 2.5 μm [1].

This HS technology is reported to have the potential to provide superior target to background discrimination, when compared to equivalent spatial resolution single-band devices. HS systems have several potential advantages over multispectral and single band systems. They have the capability of detecting targets of sizes smaller than an individual pixel. They also have the ability to identify a target/feature based on its chemical constituents' reflectance properties. This procedure requires the comparison of an image pixel's spectrum with material reference spectra and matching spectral features to allow identification. This technique is used by the mining industry to locate mineral deposits. [2,3]

HS technology is finding application in a range of areas under a broad umbrella of activities, including environmental monitoring, surveillance and mineral exploration. Investigations into the phenomenology of land mine detection, camouflage detection and identification, and intelligent missile seeking [4,5,6] as well as chemical plume detection for battlefield monitoring [6] and pollution detection from industrial facilities [7,8] are but a few examples of potential uses.

1.2 Aims

The objective of this report is to investigate issues affecting the ability to detect targets of interest against various backgrounds, by the application of remotely sensed radiance information at hyperspectral resolution. This investigation is based on high resolution spectral signatures, upon which 'forward modelling techniques' are applied to incorporate the effects of the sun-sensor geometry, the atmosphere and the sensor's characteristics in modulating this information.

This report aims to investigate phenomenology issues including the measurement of material reflectance, atmospheric propagation effects and the application of atmospheric modelling tools. It also aims to provide analysis procedures and approaches to exploit modelled results.

The purpose of this report is not to provide a definitive answer to hyperspectral band selection issues, nor quantify solutions to the detection performance enhancements expected by using hyperspectral techniques, but more to outline appropriate approaches and identify issues which need attention when considering a hyperspectral sensor for surveillance purposes.

1.3 Scope

The target and background combinations, sensing geometry and atmospheric conditions that have been employed in this study are guided by a desire to apply scenarios congruent with the JP-129 task. The scenario employed corresponds to a sensor/airborne platform flying at 2.5 km altitude with nadir viewing geometry. A list of targets and backgrounds for which spectra were investigated is provided in Table 1.1.

Table 1.1. Targets and backgrounds investigated.

TARGET CLASS	
Target	Background
Aluminium dinghy	Eucalypt (*E miniata & E tetrodonta*)
Blue inflatable boat	Leaf Litter
Green camouflage	Mangroves
Red vehicles	Melaleuca
Military vehicle	
White fibreglass boat	
White vehicles	

The scope of the study has been confined to the comparison of reflectance spectra of targets and backgrounds in Table 1.1, the modelling of the radiance arriving at a given sensor, (assuming appropriate environmental conditions) and the modelling of this sensor's outputs.

The AVIRIS (Airborne Visible-Infrared Imaging Spectrometer - Jet Propulsion Laboratory, USA) hyperspectral sensor's performance has been modelled in this study [9]. Predicted 'at-sensor' radiance spectra were converted to corresponding digital number outputs by the application of the AVIRIS sensor's spectral response functions and radiometric calibration coefficients.

In this study the performance of two moderate resolution, radiative transfer modelling packages have been compared.

2. Modelling Methods

2.1 Acquisition of Spectra

To completely characterise a material's reflectance spectrum measurement of both the diffuse and directional reflectance components are required. These components are highly wavelength dependent. When surface irregularity or roughness is less than the wavelength of light specular reflections dominate and vice versa when surface irregularities are randomly orientated and larger than the wavelength of light being considered. Generally most natural materials are diffusely reflecting in the visible region of the spectrum. [10]

While many of the materials discussed in succeeding sections can demonstrate significant specular or directional reflectance components, the scope of this study has been limited to diffuse surfaces only. The primary focus is on the material's spectral colour rather than its surface texture. This avoids the difficult and somewhat problematic determination of Bi-directional Reflectance Distribution Functions

(BRDF) needed to characterise the directional components of a material's reflectance spectrum.

As fundamental physics determines that molecules can only absorb and emit light at discrete quantised levels, it follows that the spectral absorption features of any given material are clearly determined by the material's chemical composition. The position and intensity of these features can therefore be used as a 'fingerprint' to aid in materials' identification. These absorption features arise from electronic, vibrational or rotational transitions within a material. The electronic absorption of chlorophyll in the visible band (0.35 to 0.75 μm) and the vibrational stretch overtone of water at 1.38 μm are two significant examples of these processes. More extensive fundamental discussions in this area can be found in many good spectroscopy texts, such as Banwell [11] and more applied discussions in much of the remote sensing literature. [12]

2.1.1 Comparison of Laboratory and Field Based Spectra

To determine the accuracy and robustness of the spectra collected in the field comparison was made with those obtained from the same material in a controlled laboratory environment.

A white canvas sample was employed in this comparison, although any of the target or background classes would have been suitable. The material used was a heavy grade polyester/cotton canvas blend. No obvious glint or 'shiny' reflection was seen when viewed from a wide variety of angles and different illumination sources, with the sample maintaining its uniform matt colour. The weave of the fabric was expected to afford only minor (if any) variation in directional reflectance properties of the material over the wavelength region of this study.

Field based reflectance spectra for this study were obtained using an Analytical Spectral Devices, Inc., (ASD) FieldSpec® FR spectroradiometer. This device is available to DSTO for a two week period each year as part of a collaborative agreement between a consortium comprised of DSTO, CSIRO, the University of New South Wales, the University of Wollongong, the Australian National University and the Charles Sturt University. This compact portable system allows rapid spectral sampling from 0.4 to 2.5 μm. The full-width-half-maximum (FWHM) resolution is 3 nanometres (nm) for the region 350 – 1000 nm and 10 nm for the region 1000 – 2500 nm.

A Varian Cary 5E UV-Vis-NIR spectrophotometer with a diffuse reflectance accessory was used to collect spectra in the laboratory for comparisons. This device was calibrated against a known HALON (Poly-Tetra-Flouro-Ethylene) standard. The standard's reflectivity was greater than 99% in the 350 to 1800 nm region and greater than 96% for the remainder of the useable spectral range between 200 and 2500 nm. The data was acquired at 1 nm sampling intervals with a spectral bandwidth of 2 nm. While this device can acquire spectra at much higher resolution (down to

0.02 nm data intervals), the data presented was satisfactory to allow for a comparison with the field-based data.

The measured reflectance values were recorded relative to standard reference plates and were not corrected to absolute values. The reference plate used in the laboratory was measured to have approximately 2 to 3% greater reflectance than that used for the field based measurements, presumably due to soiling and environmental exposure of the latter. This bias is expected to result in a small increase in the relative reflectance values measured in the field, but is not expected to be significant when compared to other sources of variability.

Two sets of field spectra of the white canvas were collected using the ASD, each set comprised, 4 and 7 spectra respectively. The first set was collected with viewing angles close to nadir, with the reference panel placed at the same position from the collection optics as the sample. The second set was taken from a variety of viewing angles, with the reference panel not always in the same position as the white canvas target. This second scenario was more representative for the collection of field spectra of the more complex targets due to the often, limited access to, and variable orientations of these targets and backgrounds.

Several spectra were recorded with the Cary instrument under controlled laboratory conditions. The mean values of these measurements and the ASD field measurements are illustrated in Figure 2.1. The Cary based laboratory spectra were uniform and displayed only minor variability between spectra. The average results accurately represented the majority of the data collected.

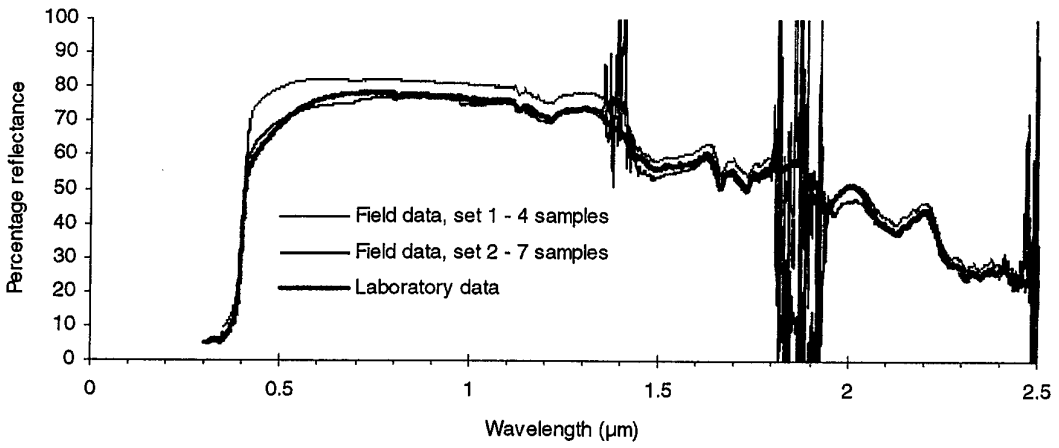

Figure 2.1. ASD Field spectra and Cary 5E laboratory spectra of white canvas.

The position of spectral features from both ASD and Cary spectrometers are consistant, although some anomalies are observed in the field based data. Centered at 1.38 and 1.85 μm are regions of considerable noise. This is associated with strong

attenuation of solar radiation due to atmospheric water vapour. The very small signals collected in these regions are swamped by the ASD's intrinsic system noise. Water vapour absorption is also expected to influence the spectra from approximately 2.35 to 2.5 μm, as well as less significant features centered around 1.14 and 0.94 μm. The spectral data becomes progressively noisier at longer wavelengths. This is due to normal reduction in radiance of the illumination source (namely the sun) resulting in a reduced signal from the sample, and hence a greater contribution due to the baseline system noise. A sharp edge was also observed in several of the individual ASD spectra near 1.0 μm, this feature marks the change-over point between the ASD's detector systems, as they were not properly matched for all the data presented here. This has the potential to introduce false results in this region for this data. Generally, careful system optimisation during data acquisition should avoid this problem.

While the mean of the field-based spectra in set 1 displayed satisfactory agreement with the laboratory-based results, individual spectra differed by up to 15% of the mean in selected bands. This variablity is illustrated in Figure 2.2. The reflectance measurements recorded in set 2 of the field data were all greater than the lab based data. This trend was seen for other target materials. Due to the different geometry used in set 2, the propagation path between target and the ASD was greater than that between the reference and the ASD, and the target was viewed at an oblique angle while the reference was held normal to the collection optics. These variations resulted in greater along path scattering and a target that was effectively larger with respect to the reference than the set 1 case. Both of these differences were expected to increase recorded reflectance values.

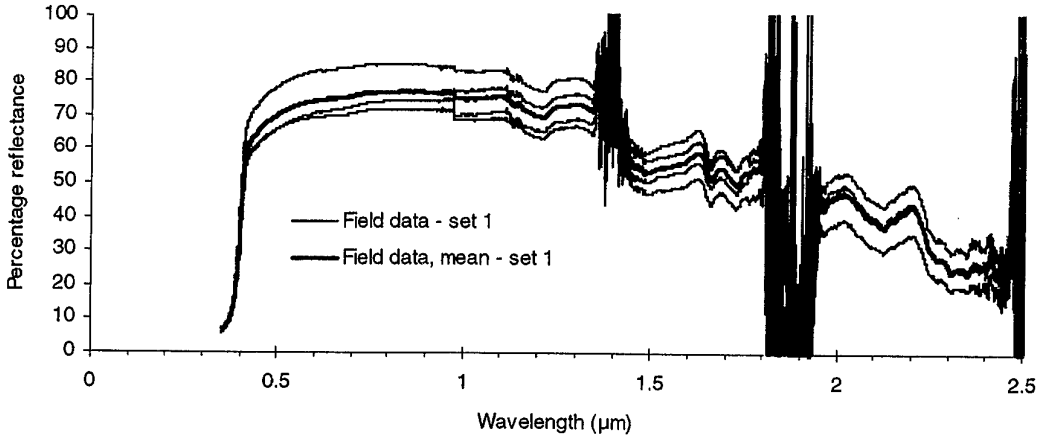

Figure 2.2. Variability in set 1 of the ASD field spectra of a white canvas sample

Overall the field-based data displayed significantly greater variability than the controlled laboratory data. While in principle the reflectance of a material is fixed and invariant of external factors, this study illustrates the dynamic and variable nature of field spectroscopy. It is important to acknowledge parameters including

the time of day, solar zenith angle, azimuth angle of the detector, aspect of the reflecting surface, nature of surrounding vegetation, distance of operator from collection aperture, etc., can and often do have significant effects on the recorded spectra. [12,13,14]

In summary, the reflectance spectra employed in this report cannot be assumed as absolute values for these materials. It appears target and background spectra display similar biases and the positions of the spectral features are accurate; this indicates meaningful comparisons are still possible. The assessment of target detection ability used in this report was based on exploiting the qualitative characteristic spectral 'finger print' of a target material with respect to background rather than a quantitative analysis approach.

2.2 Atmospheric considerations

Spectral radiant energy passing through the earth's atmosphere is subject to absorption, emission and scattering by the atmosphere's constituents. The extent to which this occurs is dependent on local atmospheric conditions including the variability and characteristics of aerosol and particulate materials, and the wavelength of light being considered. Thus a remotely sensed spectral radiance signature of any target will have its character significantly modified of due to the influence of the atmosphere. This modification is independent of the target or the background properties.

Any simulation software that attempts to 'forward model' the predicted spectral radiance at a sensor must include all the pertinent atmospheric parameters discussed above, along with accurate sun, target and sensor viewing geometry. The package must also incorporate reflectance data of the materials of interest, at the spectral resolution commensurate with the sensor and the spectral features of targets and backgrounds.

The Modtran [15] (Moderate resolution code for Lowtran) software developed by the now Phillips Laboratory/Geophysics Directorate has been demonstrated as suitable for atmospheric propagation and radiance modelling. Modtran is one of the most widely distributed and validated codes available [15-18]. The Mosart (Moderate Spectral Atmospheric Radiance and Transfer) package is another candidate. This code has evolved from similar precursors as those of Modtran, with many in-built features and profiles being conserved. Mosart includes all the Modtran atmospheric features and is easily applied to any arbitrary line-of-sight calculations as required for this study. Both Modtran and Mosart are 1 cm^{-1} 'spectrally-binned' band model codes as discrete from the high-resolution 'line-by-line' alternatives like Fascode [18,19] that consider all molecular absorptions. Both Modtran and Mosart have a maximum defined resolution of 2 cm^{-1}. This resolution is well in excess of what is required for modelling in hyperspectral space. For example, 1 cm^{-1} at 1.0 μm corresponds to a resolution of approximately 0.1 nm. A spectral resolution of about 10 nm and a spectral sampling interval of approximately 2 to 3 nm has been

specified as a minimum requirement for hyperspectral remote sensing applications in the 0.4 to 2.5 μm wavelength region. [20]

The units of wavenumber or reciprocal centimetres (cm^{-1}) are often used by spectroscopists and can be converted to wavelength by simple inversion and multiplication by the appropriate scaling factors.

It is noted that neither Mosart nor Modtran provide information about any statistical variability that would be encountered under normal operational conditions. The source of this variability is complex, with parameters including pressure, temperature, humidity and visibility all contributing. This variance is difficult to model because of the many undefined variables. Thus experimental measurements would provide the ideal source of this variance data. Such experimental measurements would also provide validation (or otherwise) to the modelling predictions.

2.2.1 Comparison between Mosart (Hypex™) and Modtran (ver 3.5)

Atmospheric propagation and radiance modelling was performed using the Hypex™ (Hyperspectral Exploitation Toolkit) software package. This package has been developed by Photon Research Associates, Inc.. It uses an embedded version of Mosart 1.41 to perform the atmospheric radiance and propagation calculations. The toolkit allows a 'user friendly' exchange of reflectance data and radiance results.

With Hypex (Mosart) being a relatively new package, comparison with Modtran was performed to provide an indication of the consistency of the radiance results generated. The Modtran code has been regularly applied to 'point-to point' (ie line-of-sight) atmospheric radiance and transmission modelling and has been demonstrated to show agreement with experimental results [18], thus ideally close correlation with Mosart is desired. While it is acknowledged this approach does not provide an independent verification, it is still a useful test within the limits of the code's accuracy.

Many of the atmospheric composition and climatic characteristic profiles used in these codes are conserved. This presents a relatively easy input selection to allow for comparisons to be made. Basic input variables were set to 'Tropical Annual' constituents profile, 'Rural' boundary layer aerosol profile and a meteorological range of 23 km. The Sun's zenith angle was calculated to represent a site in Darwin at 12:00 noon local time on January 1. The viewing geometry was chosen to be 2.5 km looking at nadir and was corrected for surface elevation. A 100% diffuse reflecting surface, at ambient temperature was employed as the target. The results of this test are illustrated in Figure 2.3.

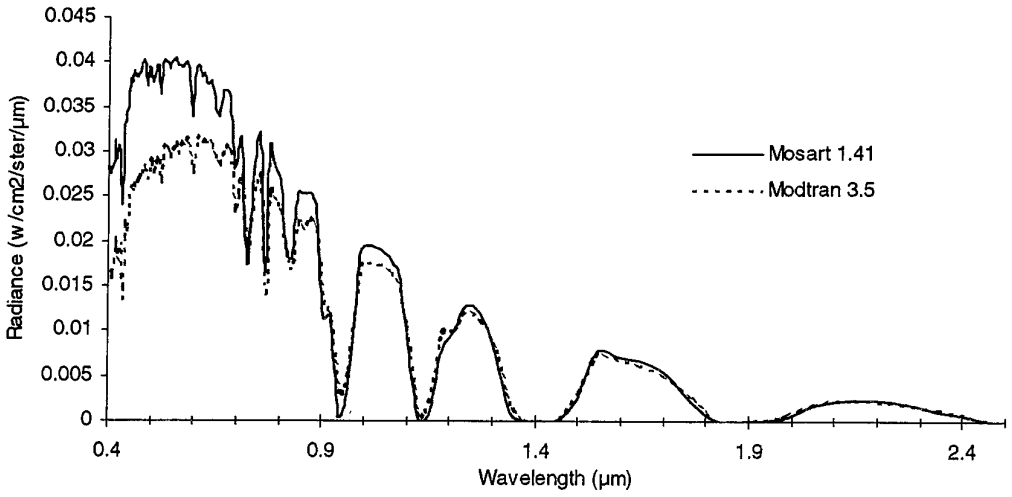

Figure 2.3. Comparison at the sensor between Modtran ver3.5 and Mosart 1.41 (Visibility 23 km rural aerosols and tropical atmosphere)

The results displayed in Figure 2.3 depict radiance differences between the two codes, with the discrepancy more pronounced at shorter wavelengths. The absorptive structure of the spectral radiance data appears well correlated; thus the disparity was expected to be associated with how the codes deal with aerosols and/or scattering computations. Further modelling was conducted to test this conclusion.

While Modtran allows computations to be performed in the absence of aerosol effects, Mosart does not. To circumvent this problem an unrealistically high boundary layer visibility of 200 km was employed for these calculations. Generally aerosol effects in the troposphere and stratosphere are negligible in comparison to the 0-2 km boundary layer aerosols. They are therefore not expected to contribute substantially to the overall attenuation in this investigation and hence do not need modification. This assumption is supported by the data depicted in Figure 2.4, where agreement is obtained between the atmospheric molecular absorption predictions generated by the two codes.

As the aerosol profiles used in each of the codes are identical, the discrepancy is associated with the scattering routines. Correspondence with the code suppliers has indicated their awareness of these differences [21,22] and it is expected that the later versions of this code will clarify this discrepancy. It was suggested that caution should be employed when using results generated employing Mosart ver 1.41 due to the uncertainty of their accuracy. [23]

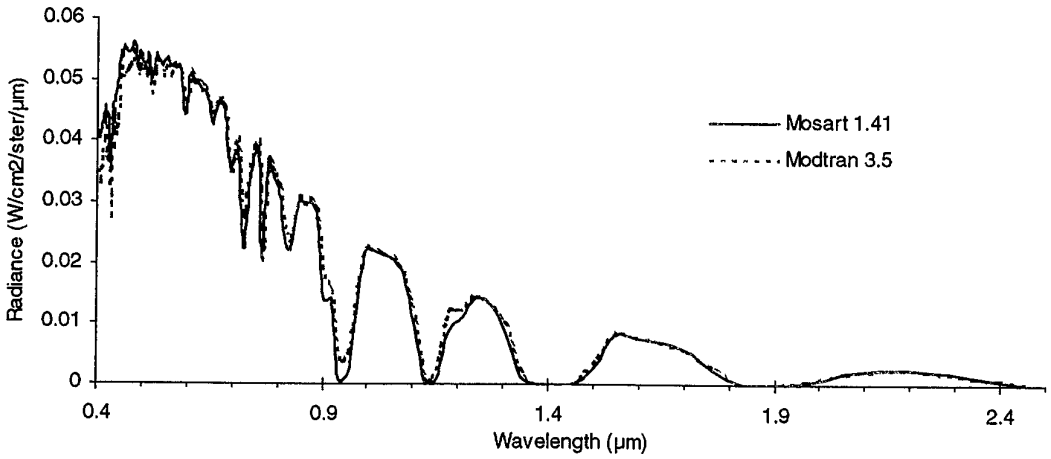

Figure 2.4. At-sensor radiance comparison between Modtran3.5 (No Aerosols) and Mosart (visibility 200 km)

The Mosart code normalises the atmosphere's molecular species concentrations when accounting for trace constituents, (Modtran does not) and also employs a modified Koschmieder formula [15] that is stated to more accurately describe hazy scenarios. Thus while it is suggested Mosart may be more reliable in poor visibility conditions [22] further validation is clearly required.

It has been reported the Modtran 3.7 and the Mosart 1.60 beta codes have demonstrated a transmittance difference of less than 0.01%, a single scatter difference less than 10% and a multiple scattering difference somewhere between 20-50% [22]. As the calculations presented in this report are based on a 23 km standard clear visibility scenario, the effects of multiple scattering on results will be negligible.

In summary, the predicted 'at-sensor' spectral radiance values must not be considered as absolute values. The only way to address these validity issues is to conduct 'in-the-field' investigations to determine which code, conditions and parameters best describe actual operating scenarios. At present these validity measurements are beyond the scope of this investigation. Even with the problems identified above it is still possible to make comparisons between targets and backgrounds, based on these predictions. This is because data generated for both targets and backgrounds will have the same bias due to atmospheric effects.

2.2.2 Comparison of 'Atmospheric Model Profiles' and Site Specific Data

A comparison was made between the Mosart predicted 'at-sensor' radiance values, incorporating site specific pressure, temperature and humidity vertical atmospheric

profiles for Darwin (as obtained from the Bureau of Meteorology - National Climate Centre), and that from the in-built 'Tropical' profile. Only relatively minor discrepancies were observed between the results. While this test indicates that the small differences in the atmospheric constituent profile is not a dominant factor affecting modelling accuracy, significant changes in the results are expected under the influence of localised humidity, visibility and aerosol variability. These properties vary with time for any given site and are difficult to model precisely.

In conclusion, it is acknowledged that some of the specified parameters, including default atmospheric constituent and aerosol profiles may not be absolutely accurate for conditions expected in Darwin on the first of January. However, it is still possible to make worthwhile comparisons between targets and backgrounds, by application of these representative profiles and models, along with site specific meteorological information.

2.3 AVIRIS Sensor Simulation

After simulating 'at-sensor' spectral radiance values for a variety of targets and backgrounds these outputs were then converted into AVIRIS sensor outputs. The aim of this process is to see if the targets can be detected by a 'state of technology' sensor.

The AVIRIS sensor was chosen as a representative example of a current leading-edge hyperspectral system. An advantage of using this system is the availability of pertinent sensor characteristics needed to model its performance. Parameters such as spectral response functions, band position, band-width, Noise Equivalent Radiance (*NER*) and radiometric calibration coefficients were all available in the open literature, or from the Jet Propulsion Laboratories, USA (JPL). An altitude of 2.5 km was employed for the simulation. This altitude affords a ground based pixel size approximately commensurate with the primary targets (small boats and vehicles) of interest.

The simulation of AVIRIS data was accomplished by passage of the simulated radiance spectra through a two-stage algorithm. Radiance data was firstly convolved with the sensor's spectral response functions. The spectral response function for all AVIRIS bands was assumed to be Gaussian with the band-pass fully defined by the band-centre positions and their Full-Width-Half-Maximum (FWHM) values. Using this band-pass information the total energy (W/cm2/sr/μm) per channel was derived from the modelled radiance spectra. The convolution process is graphically demonstrated in Figure 2.5.

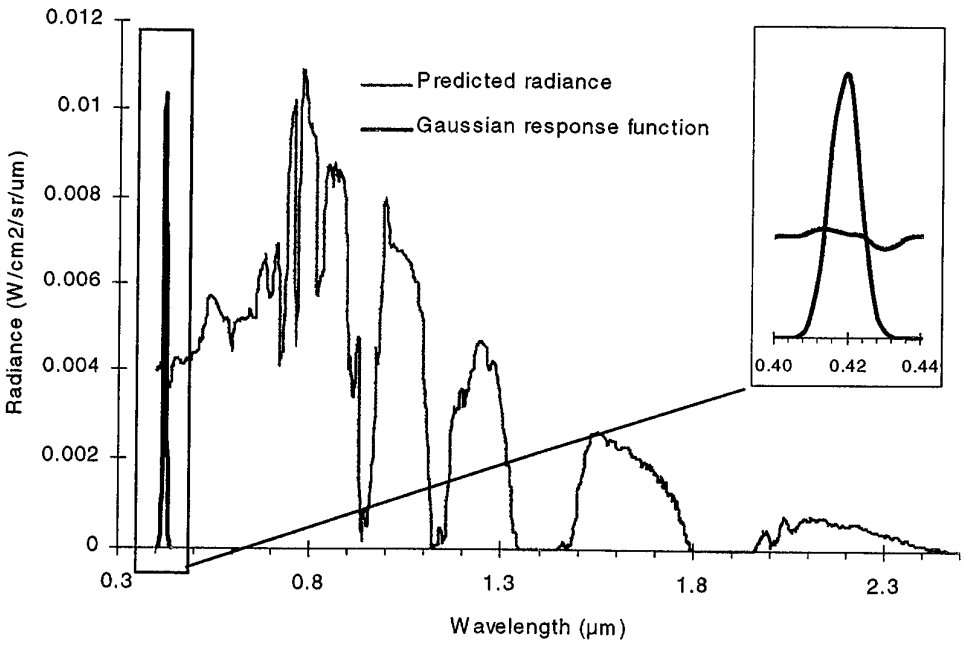

Figure 2.5. Example of sensor response function integrated with an at sensor radiance spectra for a military vehicle, function centred at 0.42 μm.

The radiance data generated from the Mosart software (Hypex) had a spectral sampling interval of approximately 3nm, which is significantly greater spectral resolution than the AVIRIS sensor's Gaussian band-pass of 10nm. This provides in excess of eight sampling points for each band pass and is satisfactory for hyperspectral analysis [20].

In the second stage, the integrated radiance signal (total in-band energy) for each channel was converted to digital number (DN) values by the application of known radiometric calibration coefficients. This process was applied to all 224 AVIRIS channels from 0.4 to 2.5 μm.

3. Analysis of Spectra For Band Selection

3.1 Overview of Single and Multiple Band Spectral Analysis for Target Detection

For single broadband sensors, target detection against background clutter relies primarily on target intensity and textural contrasts. Shape also plays a major role and hence high spatial resolution becomes a requirement to detect, recognise and identify targets. In contrast hyperspectral sensing aims to exploit the spectral

differences between a target and the clutter to aid in detection and (potentially) recognition. While target-to-clutter ratios (*TCR*) may often be low in many or all hyperspectral bands, analysis of two or more bands simultaneously can often significantly increase the *TCR*. This can provide improved detection of targets with a reduced false alarm rate, with an added advantage of often-lower spatial resolution requirements. [1]

The primary method of hyperspectral signature processing employed in this report is based on single spectral-band processing. The current analysis has been aimed to determine a 'first-cut' likelihood of discriminating targets from backgrounds. While there is scope for complex multiple band (multivariate) data analysis when processing this hyperspectral data, only a single case has been provided as a demonstration of this approach. Due to the small number of signatures available in this analysis a robust multivariate approach was not possible.

This single band approach is aimed to allow for 'fast filtering' of data sets. The aim is to identify regions of interest before more complex multiple band procedures, with their corresponding overheads in time, computing and resources are employed. As hyperspectral sensors have the potential to generate massive volumes of data, this approach has the advantages of significantly reducing the analyst's workload by targeting spectral bands of high utility while ignoring the less useful chaff.

3.2 Single Band Analysis

For initial single band processing where the target or background is larger than a given pixel's instantaneous-field-of-view (*IFOV*), the target-background radiance difference can be defined by equation (3.1)[1]

$$\Delta L^S = \frac{(L_T - L_B)A_{IFOV}e^{-\tau.d}}{d^2} \qquad (3.1)$$

Here L_T and L_B are the target and background radiance values, respectively, L^S denoting 'at-sensor' radiance values A_{IFOV} the area of the *IFOV*, τ the atmospheric transmission coefficient and d the distance from the sensor to the scene. As the Mosart atmospheric propagation and radiance code computes the radiance at the sensor by taking into account the variables in (3.1) we can simplify the equation to

$$\Delta L^S = L_T^S - L_B^S \qquad (3.2)$$

The effect of system noise on the detection ability of a given target can then be defined by the signal-to noise ratio (*SNR*) below [1]

$$SNR = \frac{|\Delta L^S|}{NER} \qquad (3.3)$$

Where *NER* is the spectrally dependent noise-equivalent-radiance of the sensor system (refer forward to section 4.8).

This *SNR* value provides a measure of target detection ability assuming that there are no variations in the signatures (radiance values) received from targets and backgrounds. This assumption does not hold true 'in-the-field' and for that reason a 'target-to-clutter-ratio (TCR^2) can be defined that includes this variability. This parameter is described as

$$TCR^2 = \frac{(\Delta L^S)^2}{(\sigma_T^2 + \sigma_B^2)} \qquad (3.4)$$

Here ΔL^S is the difference between the mean signatures of the background and target classes, and σ_T and σ_B are the sample standard deviations of the background and target classes. The TCR^2 is a measure of the separability between target and background and it is the same measure as Fisher's criterion [24] for class separability. The relation (3.4) assumes that the target and background samples are independent and are normally distributed. [1]

While the equations described above deal with at-sensor radiance, an entirely analogous protocol can be employed in processing measured reflectance data or the digital outputs of a given hyperspectral sensor.

3.2.1 Dealing with Small Sample Sizes

When the number of samples for targets or backgrounds employed in an analysis is small (<30), which is the case in this study, an analysis that does not make allowance for the effects of sample size may be inaccurate. To account for this small sample case a modified TCR^2 measure can be derived as described by

$$TCRs^2 = \frac{(\Delta L^S)^2}{\left[\frac{(n_T - 1)s_T^2 + (n_B - 1)s_B^2}{(n_T + n_B - 2)}\right]} \qquad (3.5)$$

Where n_T and n_B are the number of samples in the target and background classes and s_T and s_B the target and background sample standard deviations respectively. This equation provides weighting based on the number of samples in each class. The $TCRs^2$ statistic is implicitly based on the assumption that the target and background distributions are Gaussian or close to Gaussian: under this assumption the $TCRs^2$ statistic will have an approximately *"Chi Square"* distribution.

Even with this weighted approach ideally sample sizes greater than 30 should be employed (if available). This allows more accurate determination of statistical estimates.[25]

The $TCRs^2$ measure is particularly useful in the initial data analysis. It provides a fast means to determine and identify spectral regions of interest for target detection. This information can then be employed in alternate approaches to allow for determination of performance indicators such as receiver operating characteristic (ROC) curves.

3.2.2 Likelihood-Ratio Detection

With the desire to extend beyond the $TCRs^2$ analysis, an alternate 'likelihood-ratio method' approach can be employed ideally after specific regions of interest have been identified. This approach requires an assumption of both the target and background displaying a Gaussian distribution, and provides a well-defined solution for ROC curves. A more formalised description of the approach employed in this report can be found in the 'Military Utility of Multispectral and Hyperspectral Sensors' prepared by Anderson *et al* [1].

In this approach a target or background population can be described by the Gaussian distribution function (3.6)

$$f(x) = \frac{1}{\sqrt{2\pi}\sigma} e^{-\frac{1}{2}\frac{(X-\mu)^2}{\sigma^2}} \qquad (3.6)$$

Where μ and σ are the mean and standard deviation respectively.

If a target and background population can be described by the functions $f(x|T)$ and $f(x|B)$ then a likelihood-ratio test, can then be applied to determine threshold levels as illustrated by the relationship [24]

$$\frac{f(x|T)}{f(x|B)} \begin{matrix} > \\ < \end{matrix} threshold \qquad (3.7)$$

This ratio returns a value that can be employed as a *threshold* to determine a probability of detection (Pd) and probability of false alarm (Pfa). The Pd can be calculated by integrating $f(x|T)$ for all values of x for which the ration in equation 3.7 is greater than or equal to the threshold, with the Pfa determined by integration of $f(x|B)$ over the same range. If this process is applied over an appropriate range of thresholds, a Pd verses Pfa ROC curve can be derived.

3.3 Multiple Band Analysis

The use of multiple spectral bands in a given target and background population provides the potential for a more powerful analysis approach to the single-band processes outlined earlier. This approach is analogous to that presented in Section 3.2.2 and is expected to significantly enhance target detection performance when the multiple bands selected are significantly correlated, as they often are. [1]

This approach can be readily extended to include whatever number of bands is required or available. The only limiting factor being the number of samples available to estimate statistical parameters such as mean vectors and covariance matrices of materials. If N bands are chosen at least N(N+1)/2 samples are needed. This requirement for large spectral libraries often provides limits on the number of spectral bands that can be effectively employed, as it is often difficult to obtain such large numbers of spectra for materials.

A covariance matrix can be assigned for a given target or background population comprising k bands as illustrated

$$\begin{bmatrix} \sigma_{11} & \sigma_{12} & .. & \sigma_{1k} \\ \sigma_{21} & \sigma_{22} & .. & .. \\ .. & .. & .. & .. \\ \sigma_{k1} & .. & .. & \sigma_{kk} \end{bmatrix} = \mathbf{C} \qquad (3.8)$$

A population distribution function analogous to equation (3.6) can then be assigned for both the target and background. This probability distribution function is given as

$$f(\mathbf{x}) = \frac{1}{(2\pi)^{\frac{N}{2}} |\mathbf{C}|} e^{-\frac{1}{2}(\mathbf{x}-\mu)^T \mathbf{C}^{-1}(\mathbf{x}-\mu)} \qquad (3.9)$$

Here x is a spectrum (vector) of N bands, C is the covariance matrix of x, and μ is the mean vector. |C| is the determinant of the covariance matrix C. The equivalent of the $TCRs^2$ of (3.5) in multivariate space is given by the Mahalanobis distance [26,27] as described by equation (3.10).

$$TCR^2 = (\mu_T - \mu_B)^T \left(\frac{\mathbf{C}_T + \mathbf{C}_B}{2} \right)^{-1} (\mu_T - \mu_B) \qquad (3.10)$$

Here μ_T and μ_B are the mean vectors of target and background and C_T and C_B the covariance matricies of target and background respectively. A likelihood-ratio test

can be performed on chosen target and background distributions, and a Pd and Pfa determined for each selected threshold value.

An analysis is presented for a two-band example; the results are presented graphically in Section 4.5. The primary difference to the single band analysis being the integration was performed over two ranges instead of one. This can be visualised by thinking of integrating over volume rather than area.

4. Results and Discussion

The *TCRs*[2] and single and multiple band Likelihood-Ratio analyses presented in succeeding sections are based on simulated AVIRIS digital number values.

4.1 Target and Background Reflectance Spectra Comparisons

All the reflectance data used in this report were collected using the ASD spectrometer in the field. Issues relating to acquisition of these spectra can be found in Section 2.1. The mean reflectance spectra of the materials investigated are all illustrated in Appendix A. These targets and background are a preliminary set, and were selected to represent three main groups. The first group is a set of terrestrial based targets (vehicles and camouflage), the second is a variety of small boats (littoral targets), and the last is a set of natural backgrounds.

From a cursory examination of the reflectance data, many spectral features can be identified, and at a first glance, many features should be exploitable for spectral detection and identification. Spectral regions where the materials are strongly absorbing or highly reflecting are clearly evident, along with regions where there are large reflectance changes over small spectral ranges. These rapidly changing 'edge' regions are also often used for identification. The positions of some of these spectral features are summarised in Table 4.1.

Table 4.1. Spectral features of targets and backgrounds

Target/Background	Spectral position (nm)	Description
Military vehicle	410, 550	Peaks corresponding to blue and green components in paint
	750	'red edge' position of paint
	810	NIR reflectance peak
Green camouflage	810	'red edge' position of material
Red vehicles	650	Red reflectance peak characteristic of material
Blue inflatable boat	470	Peak due to blue component in paint
Eucalypt	460, 550	Peaks associated with chlorophyll and other leaf components
	720	Chlorophyll 'red edge'
	1450	Liquid water absorption

While not all the significant spectral features have been highlighted, just from the data presented many of these materials can be identified based on colour. For example, with lower spectral resolution data, (10's of nm) we can assign whether a target is blue or red based on the peak/edge features at 470 and 650 nm respectively. At higher resolution (5 to 10 nm) it should be possible to identify the difference between the green plant backgrounds and green paint/green camouflage based on the characteristic green reflectance peaks at 540-550 nm for targets and 560 nm for the vegetation background. The chlorophyll 'red edge' of these plants at 720 nm as compared to the 'man-made' targets 750/810 nm features could also be employed to discriminate between the classes.

Not only are peak and 'edge' reflectance positions informative but absorption positions also provided considerable information about material composition. In the cases presented, mineral/man-made objects and live plant matter are clearly distinguishable. This is based on the presence or lack of liquid water absorption features at 1450 nm. This is expected to be useful in detecting camouflage designed to imitate vegetation, for as a general rule, these types of man-made materials seldom (unless wet) have liquid water absorption features.

The noise regions in the field-based data, centred at 1380 and 1870 nm, do not affect the results presented. This is due to their coincidence with the atmospheric water vapour absorption bands as addressed in Sections 2.1 and 4.2.

While an understanding of the reflectance spectra of targets and backgrounds and their associated underlying features is important, this is not what a hyperspectral sensor 'sees' or provides as outputs. Thus the analysis forming the basis of this report employed radiance values converted to AVIRIS sensor digital numbers (DNs), to determine whether it is possible to discriminate between the targets and backgrounds.

4.2 Comparison of Target and Background at Sensor Radiance Values

The Mosart (Hypex) software was used to simulate at sensor radiance data from the reflectance spectra of the targets and backgrounds displayed in Table 1.1 (and illustrated in Appendix A). The results discussed throughout this Section are based on the following geometry, location, time and atmospheric conditions.

Sensor height above the target	2.5 km looking at nadir
IFOV	2.5 m diameter (1 milli-radian)
Illumination Source	Solar (direct and scattered)
Spectral range	400 to 2500 nm
Spectral sampling interval	3 – 4 nm
Atmosphere Climatic model	Tropical (Annual)
Aerosol profiles (boundary layer)	Rural
Meteorological range	23 km
Geographical Location	S12:25°, E130:53°; Darwin, Northern Territory.
Time (GMT)	3:33.0 hrs (12:00 noon local time)
Month/Day	January 1.

As the second stage of the simulation process, all radiance spectra were converted into AVIRIS digital number signals, as described in Section 2.5. The AVIRIS DN values, generated for each target or background are illustrated in Appendix B.

The influence of the atmosphere is clearly illustrated in these results. Strong absorption bands centred at 0.94, 1.14, 1.38 and 1.87 μm (primarily due to atmospheric water vapour) result in the extinction of the sensor signal in these regions. The depth and width of these bands are dependent on the atmospheric water vapour concentration and hence relative humidity. The higher the relative humidity the greater the width and depth of the absorption bands and hence the reduced likelihood of detecting spectral features of targets or background near the shoulders of these bands.

The results presented are based on an at-surface relative humidity of 85%, representative of tropical Australia in January (when it is not raining). Under these

conditions degradation in the ability to detect liquid water absorption centred at 1.45 μm in the vegetation samples is observed, due to the adjacent 1.38 μm water vapour band overwhelming this feature. While not fully examined, an improvement in the detection of this feature is expected during drier seasons.

Many of the spectral colour features seen in the reflectance spectra can be identified in the simulated AVIRIS DN outputs (refer to Appendix B). Targets such as the white fibreglass boat can be identified as a bright target (particularly in the visible region - 0.4 to 0.75 μm). Similarly the chlorophyll 'red edge' features at 720 nm characteristic of the live vegetation samples can be seen and used for detection purposes. It becomes progressively more difficult to identify targets and backgrounds purely by visual inspection of the data when the AVIRIS DN output features correspond to only small absorption or reflectance features. The blue boat features at 470nm can be identified with priori knowledge of what to look for, but to discriminate between the green vegetation, green camouflage and military vehicle would be difficult using the reflectance features described in Section 4.1. Thus while dominant spectral features appear detectable, there is a low likelihood of identifying 'finger-print' reflectance features by simple visual inspection.

It is clear further data analysis and suitable target detection algorithms and post sensor processing techniques must be employed to take full advantage of the spectral information a hyperspectral sensor's output is known to contain. It is with these topics and similar performance limiting factors the succeeding sections are concerned.

4.3 Selection of Spectral Bands – $TCRs^2$ Results

The $TCRs^2$ analysis described in Section 3, has been applied to estimate the degree of difference between each pair of target and background classes chosen from those appearing in Table 1.1. Graphical representations of these analyses can be found in Appendix C. Analysis provide a case-by-case guide to the spectral regions that afford separation between target and backgrounds.

The obvious and desirable progression of the above analysis is the identification (if any) of spectral bands that provide separation against all backgrounds. The ability to discriminate a target from all backgrounds will be set by the background that defines the lower limit of the $TCRs^2$ separation. Thus a minimum $TCRs^2$ was determined for individual targets against all backgrounds, with the results being summarised in Appendix D. The lower limit on these graphs was set to one for display purposes. A $TCRs^2$ of unity or less indicates targets and backgrounds are effectively indistinguishable if only a single band is being used to discriminate between them. Although it may be possible to achieve acceptable separation with multiple band analyses even when any individual band among those being used has a $TCRs^2$ of less than unity (see Section 4.4 and 4.5).

The terrestrial and littoral target classes were considered as mutually exclusive data sets for this study. The littoral targets comprised the aluminium dinghy, blue rubber boat and the white fibreglass boat targets. The green camouflage, red vehicles, military vehicle and white vehicles were all classified as terrestrial targets. The spectral regions with the largest $TCRs^2$ value and hence greatest target/background separability were expected to be the most likely to allow target detection.

4.3.1 Littoral Targets

The spectral region between 0.4 and 0.5 μm has a superior target and background separation than other regions, for all three littoral targets. The magnitude of $TCRs^2$ measure is also at its largest for all three targets in this region. A small region between 0.55 and 0.62 μm may also be suitable, but no other region of the spectrum exhibits significant separation of all three targets from the backgrounds. Thus for this modelled scenario the recommendation for single-band target detection is to employ a sensor that operates in this spectral region.

From this data it also appears possible to discriminate between individual targets. Between 1.50 and 1.65 μm only the white fibreglass boat demonstrates significant separability against background. A region between 2.12 and 2.18 μm displays a $TCRs^2$ measure of similar magnitude only for the aluminium dinghy. Thus on the assumption this magnitude of separability (of the order of 10 or greater) extrapolates into a high probability of target detection, then a sensor system operating in the three spectral regions identified should be able to detect and discriminate all three targets using 'single-band analysis' methods. This approach is summarised in Table 4.2.

Table 4.2. Example of hyperspectral band selection to detect littoral targets against all backgrounds

Band Number	Band Position (μm)	Blue Rubber Boat Detected	White Fibreglass Boat Detected	Aluminium Dinghy Detected
Band 1	0.40-0.50	Yes	Yes	Yes
Band 2	1.50-1.65	No	Yes	No
Band 3	2.12-2.18	No	No	Yes

4.3.2 Terrestrial Targets

For the modelled terrestrial scenario no single spectral region shows significant separability for all targets and background. This example demonstrates the need for multiple bands to solve the target detection task. In this example it is assumed a $TCRs^2$ measure in excess of two to three affords satisfactory 'single-band analysis'

probabilities of detection. This is not an unreasonable assumption as will be demonstrated in following sections.

As with the littoral example, regions displaying separability from background can readily be identified. Using this information a matrix of potentially suitable spectral bands can be constructed, and by following a process of elimination a suitable suite of bands and positions can be selected to achieve the detection and identification task. A summary of this approach is depicted in Table 4.3

Table 4.3. Example of hyperspectral band selection to detect terrestrial targets against all backgrounds

Band Number	Band Position (μm)	Military Vehicle Detected	White Vehicle Detected	Red Vehicle Detected	Green Camouflage Detected
Band 1	0.40-0.43	Yes	Yes	No	No
Band 2	0.45-0.52	No	Yes	No	No
Band 3	0.60-0.64 or 0.68-0.71	No	Yes	Yes	No
Band 4	1.48-1.54	No	No	Yes	No
Band 5	2.13-2.25	No	No	No	Yes

4.3.3 Selection of Spectral Bands - Summary

The examples presented demonstrate that the individual band's position and band-pass are dynamic, and depending on target and background, the separability characteristics can vary significantly. Ideally a given band's band-pass should be set as wide as possible without losing hyperspectral information. This is because as a 'rule-of thumb' the wider the band-pass the greater the collected signal and the better the system's *SNR* performance. The examples presented were primarily designed to demonstrate this band selection approach.

These examples confirm the intuitive expectation of a greater number of sensor bands being required for target detection and identification in scenarios with greater numbers of targets.

These cases provide examples of how it is possible to develop 'training sets' of recommended spectral bands for application in mission planning. For example, if a surveillance or reconnaissance mission is planned over a littoral area, then based on the above *TCRs*[2] results, the analysis of data in the spectral band between 2.12-2.18 μm should provide an indicator of the presence of an aluminium surface against the vegetation backgrounds. Hence a sensor operating in this region would be expected to be operationally superior for this role.

While the results presented are encouraging, it must be emphasised they are preliminary, and are based on very limited data sets. Clearly in a meaningful operational role the number of targets and backgrounds will be considerably larger. Even so, when coupled with the use of appropriate 'training-data' this approach is expected to have significant potential to enhance the ADF's surveillance capability

4.4 Single Band Probability of Detection and False Alarm ROCs

With the desire to extend beyond the *TCRs*^{2} approach, an example comprising a green camouflage target and an eucalypt background was selected. ROC curves to determine target detection probabilities (Pd's) and corresponding false alarms (Pfa's) were then calculated for this case. This case was considered to be of relevance to military operations in Northern Australia. This example is the simple case of a pure target pixel alongside background. The *TCRs*^{2} determined for this example is illustrated in Figure 4.1. Other examples can be found in Appendix C.

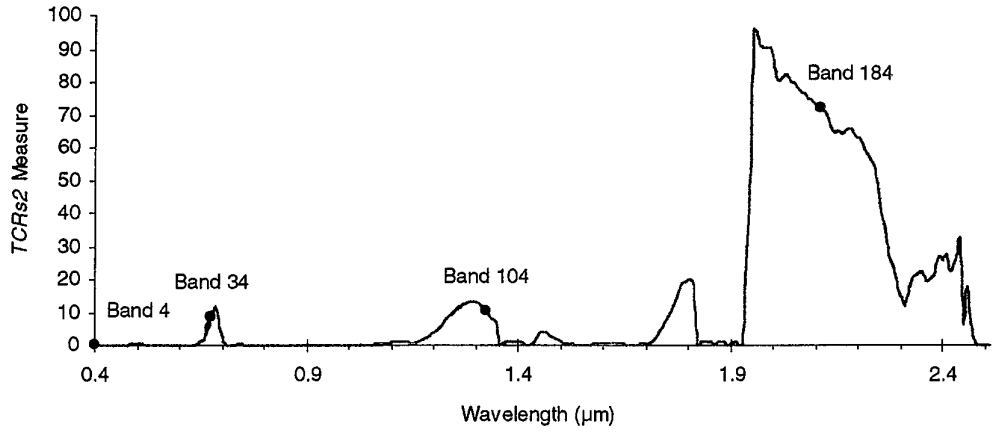

Figure 4.1. TCRs^2 *values for a green camouflage target and eucalypt background*

Four of the 224 possible AVIRIS bands (Band 4, 34, 100 and 184) were chosen for further analysis. Table 4.3 provides a summary of information about these bands. The bands were selected to illustrate the differences in the ROC curves over the range of *TCRs*^{2} values obtained for the test case.

The 'likelihood ratio detection' method discussed in Section 3.2.2. was applied to each of these four bands, with the ROCs generated illustrated in Figure 4.2.

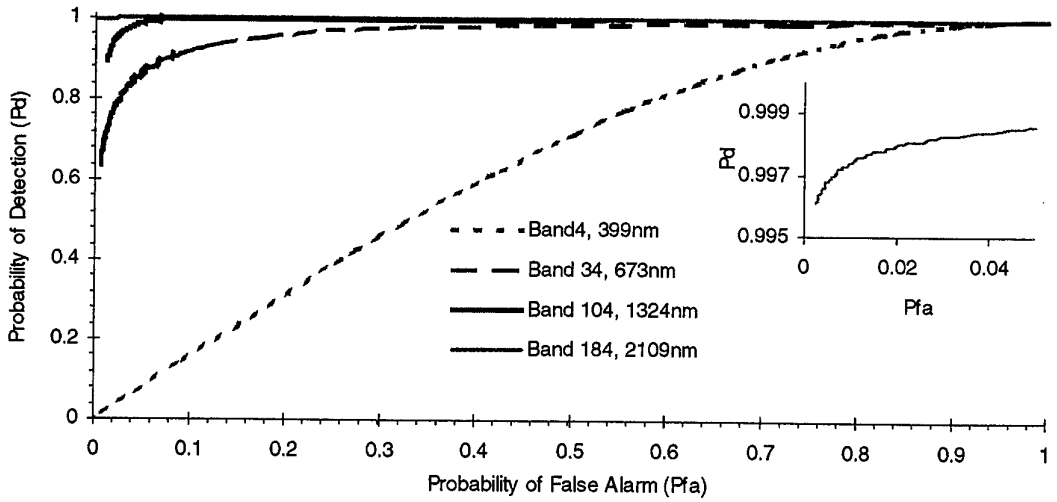

Figure 4.2. ROC Curves for AVIRIS bands 4, 34, 104 and 184 for a green camouflage target and eucalypt background.

From these results the performance differences between each band can clearly be seen and determined. The last column in Table 4.4 provides information about the approximate Pfa for a Pd of 90%. The Pfa is only approximate due to minor interpolation errors.

Table 4.4. Data summary for AVIRIS bands selected for further analysis

AVIRIS Band Number	Band Centre (μm)	Band Width (FWHM) (μm)	$TCRs^2$ Measure	Pfa for 90% Pd (approx.)
Band 4	0.399	0.00953	0.023	70%
Band 34	0.673	0.00831	8.7	7.8%
Band 104	1.324	0.01091	10.2	1.2%
Band 184	2.109	0.01078	81.5	>0.1%

AVIRIS Band 4, with its small $TCRs^2$ value (compared to other bands), has a corresponding very poor ROC curve and hence a large Pfa for any given Pd. As was expected this band is not suitable for use in single band target detection. Alternatively, AVIRIS Band 184, with its large $TCRs^2$ has a ROC curve which indicates a Pd of nearly 100% with very small Pfa values (see insert Figure 4.2). This illustrates, as expected, that this band would be highly desirable to use for target detection.

While the relationship between large and small $TCRs^2$ values and the corresponding ROC curves is clear, more ambiguity exists in determining limits for Pfa's/Pd's using

$TCRs^2$ values when they are midway between these two cases. This problem is evidenced in AVIRIS Bands 34 and 104.

AVIRIS Band 34 and 104 have similar $TCRs^2$ values (8.7 and 10.2 respectively) but have significantly different Pfa's (7.8% verses 1.2%) for a Pd of 90%. This indicates it is difficult to infer what a band's detection performance is based on the $TCRs^2$ measures alone. This is supported by analysis of other AVIRIS bands. This result relates to the different sample distributions in the target or background populations in the different spectral bands.

This sample variance is illustrated in Appendix E where the sample distributions of the green camouflage target and the eucalypt background used in the above analysis are presented. Figure E.2 and Figure E.3 illustrates the distributions of target and background (and hence overlaps) that lead to ROCs with different characteristics. Even though the $TCRs^2$ values for band 34 is within 15% of Band 104, the sample distributions have a greater overlap between target and background and hence a Pfa 6.5 times larger for a Pd of 90%. AVIRIS Band 4 displays overlap between the target and background across most the sample distribution, and hence poor ROC curves, while AVIRIS Band 184 has negligible overlap and a corresponding excellent ROC curve.

While the solution to the 'likelihood ratio detection' method and the shape of resultant ROC curves are dependent on the sample distributions of target and background, the results presented illustrate that the $TCRs^2$ values can be used (within limits) as a performance indicator guide. When $TCRs^2$ values are in excess of 10-15 there is a high likelihood of discrimination between target and background. Corresponding ROC curves are expected to show low to very low Pfa's for a 90% Pd. With $TCRs^2$ values below 1-2, reduced separation and higher Pfa's are expected. The region with $TCRs^2$ values between 2-10 has the potential for target detection with the Pfa's being dependent on the sample distributions, with the potential for significant detection performance variability.

4.5 Two-Band Probability of Detection and False Alarm ROCs

As outlined in Section 3.3, the advantages offered by hyperspectral sensors lie in the simultaneous exploitation of multiple spectral bands to improve target detection performance. This approach becomes necessary for more complicated multiple target and background scenarios in which single-band performance is generally poor.

A two-band analysis is presented, for the green camouflage target and eucalypt background example presented earlier. While this is a simple case where single band detection is possible in several spectral regions, the prime purpose is to demonstrate the performance enhancement possible by employing multiple bands.

AVIRIS Bands 4 and 34 were selected for the analysis. The approach outlined in Section 3.3 was applied to these bands. The calculated 2-band target and background sample distributions are presented in Figure 4.3. The minor contour irregularities

seen (particularly for the green camouflage) are due to limitations of the plotting procedures employed and do not affect the accuracy of the underlying analysis.

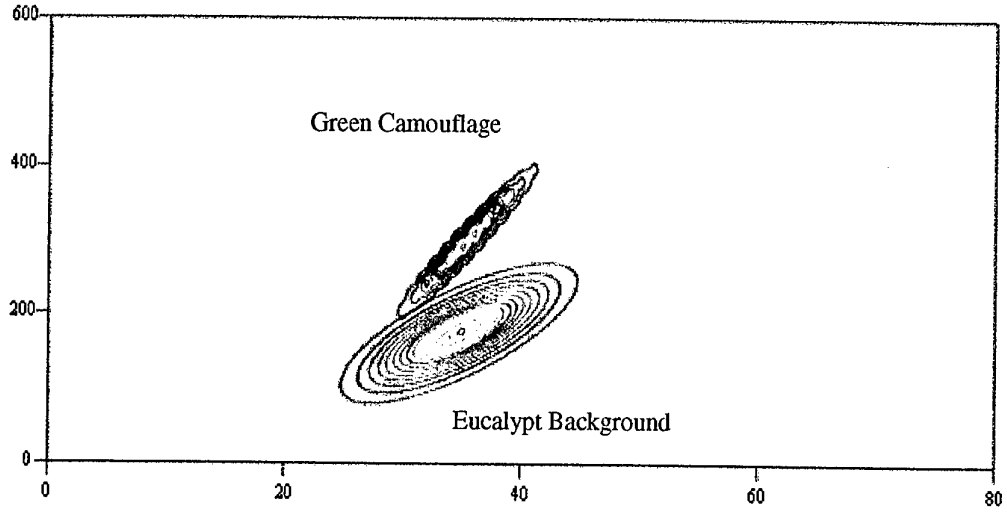

Figure 4.3. AVIRIS Band 4 and 34, 2-band anaylsis sample distributions for a green camouflage target and eucalypt background. (greatest values near the distribution centres)

From Figure 4.3 it is clear the target and background sample separation has sigificantly increased when compared to the indivdual single band cases (see Appendix E). This is manifest as a reduction in the overlap between target and background sample distributions. 'Likelihood ratio detection' analysis was then performed and the relevant volume was integrated to generate a ROC curve for this analysis. This ROC is illustrated in Figure 4.4.

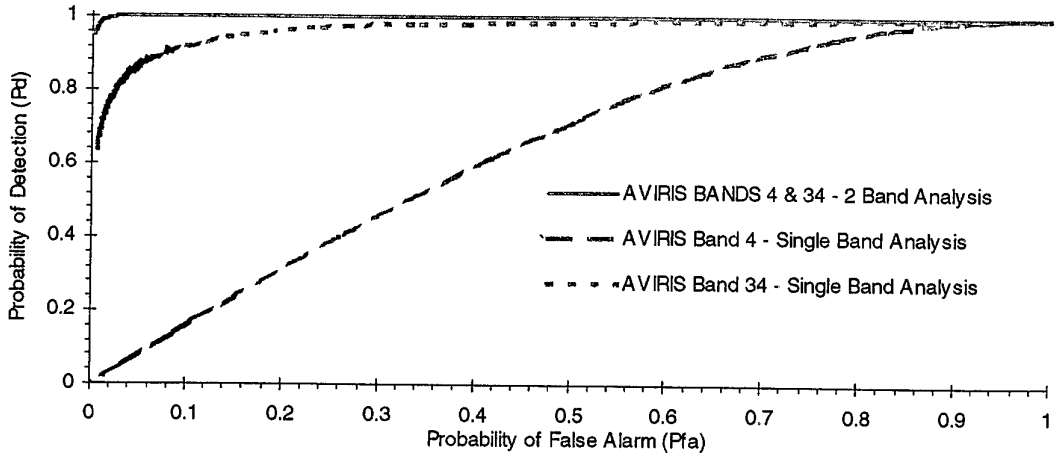

Figure 4.4. ROC Curves for single and 2 band analysis of AVIRIS bands 4, 34 for a green camouflage target and eucalypt background.

By employing this 2-band approach the Pfa for a 90% Pd has fallen from 70% and 7.8% for bands 4 and 34 repectively to less than 0.2%. This performance enhancement is even greater if more optimal AVIRIS bands are selected and/or the number of spectral bands is increased beyond 2.

This example demonstrates the huge improvements in target detection, that are possible by employing a 2-band analysis techniques. Thus multiple-band techniques are expected to be required and offer demonstratable performance enhancements when the surveillance scenario becomes more complex (and realistic) with larger numbers of targets, more complex and varied backgrounds, and 'sub-pixel' targets.

It is important to note that this case does not include the effects of 'system noise' on the detection performance, and is presented as a demonstrative example of muliple band analysis techniques only. Some 'system noise' issues and their effects are discussed in Section 4.8.

4.6 Target and Background Mixing

All previous analysis has made the assumption that the target or background of interest is larger than the *IFOV* of a single pixel and hence would contribute 100% of that pixel's signal. A 2.5 m diameter *IFOV* was used in these, and subsequent calculations, and for a majority of the targets discussed this 'pure-pixel' assumption could hold true.

This 'pure pixel' analysis was employed as it was reasoned if detection of a pure target against a pure background was not possible, then it would not be possible under less optimal scenarios. With the results generated in Section 4.3 and 4.4 indicating the potential for 'pure pixel' detection, analysis was extend to include scenarios where the target is smaller than the pixel's *IFOV*. This was expected to be operationally more realistic, where a target may occupy only a part of several pixels rather than all of a pixel. The determination of the effective 'sub-pixel' target detection limits can allow for a prediction of the greatest area a surveillance systems may be able to provide effective surveillance over, based on detector array size and viewing geometry.

The green camouflage target and eucalypt background example used in section 4.4 was used it this analysis. The target consisted of 5 spectra and the background 39 spectra. The approach taken was to apply simple linear mixing of the initial source reflectance spectra to generate 'mixed spectra' with known percentages of target mixed with background. 'At-sensor' radiance and AVIRIS DN outputs were then predicted and a $TCRs^2$ measure calculated based on the 'mixed spectra' data, using the procedures outlined in earlier sections.

While it is possible to generate 195 different target/background mixture combinations, for any given target percentage, the approach taken in this analysis was to linearly mix the background mean spectrum with each of the 5 pure target spectra. This maintains the same weighting (5 to 39) between target and background in the *TCRs*^{2} analysis, as was used in the 'pure pixel' case. This approach has significantly reduced time and resource requirements and still provides information on the effects of 'target dilution' on detection performance. It was assumed a pure background pixel was available to compare this 'mixed-pixel' against. The results of this analysis are displayed in Figure 4.5

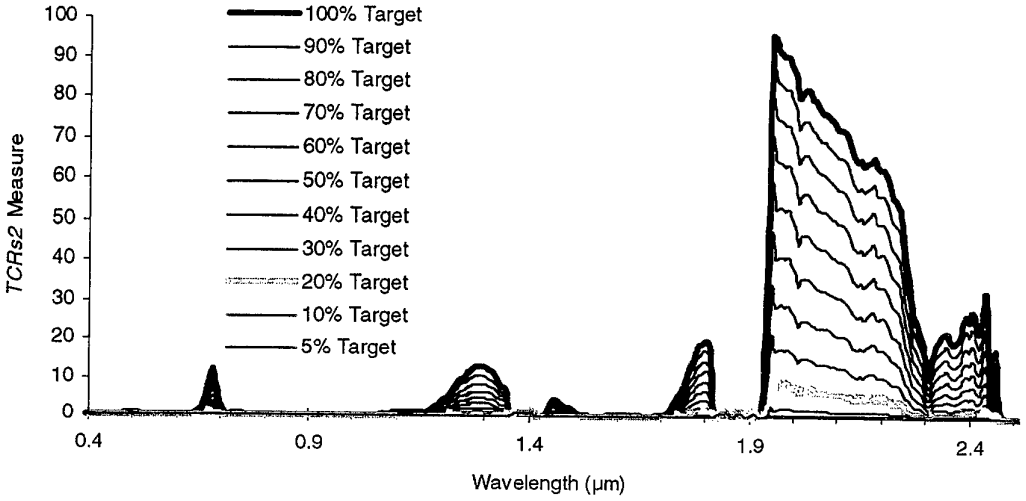

Figure 4.5. TCRs^2 *values for a green camouflage target against eucalypt background from 100% Target (greatest value) sequentially to 5% target/background mixture (smallest value)*

Atmospheric propagation effects and the sensor's spectral response characteristics are both expected to play a role in modulating the reflectance data used in this analysis. Thus while the results in Figure 4.5 appears to indicate a near linear *TCRs*^{2} reduction on the 'dilution' of target, a simple percentage comparison (to the pure target case) was performed on several of these results, to quantify the influence of these moderating factors. The results from this simple test are displayed in Figure 4.6.

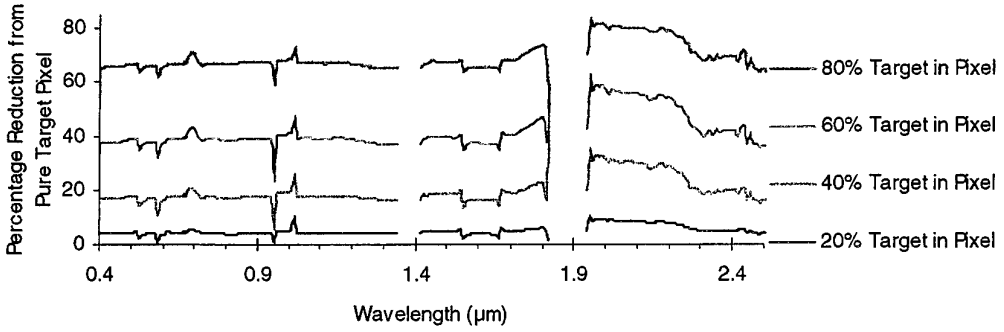

Figure 4.6. TCRs² Values percentage difference from pure target for 80%, 60%, 40% and 20% mixtures of target in background

The results in Figure 4.6 demonstrate that the effects of the atmosphere and sensor characteristics are not uniform across the spectral region of interest. It is also evident that the performance degradation is more severe for lower percentages of target in the 'mixed pixel'.

These results indicate atmospheric propagation and sensor characteristics must be taken into consideration when modelling a hyperspectral sensor's performance, with any conclusions drawn from an analysis based purely on reflectance possibly being wrong. Atmospheric propagation effects will obviously depend on meteorological conditions and sensor geometry, thus the influence of these parameters will need to be determined for each individual operational scenario.

In summary while there are several complementing factors that reduce the 'sub-pixel' target detection ability, the separation between the 'mixed pixel' and background is still the primary performance-limiting factor. Thus if the *TCRs²* is still large (>10) then high Pd's with low Pfa's should still be expected. For example, in the case presented, the spectral region between 1.95 and 2.1 μm (ie. contains AVIRIS Band 184) should still provide excellent target detection ability even with the target comprising only 20% of the pixel. AVIRIS Bands 4, 34 and 104 are not expected to be useful at this sub-pixel target level.

4.7 Geometry Considerations

Until now analysis has used a fixed time of day and sensor viewing geometry. This scenario was chosen as it provided maximum incoming solar radiation, an appropriate *IFOV* pixel size, and realistic deployment height for tactical and reconnaissance EO payloads. To extend the performance investigations further, analysis of the effects of altitude and time-of-day are presented.

4.7.1 Altitude Effects

Using the modelling approach described in Section 3.2.1, the $TCRs^2$ measure was determined for a test case employing the green camouflage target and eucalypt background. This process was performed at altitudes of 2.5, 5, 10 and 20 km, all looking at nadir. A target and background larger than a pixel's IFOV was assumed. All other parameters were held constant.

The $TCRs^2$ separation measures for all altitudes were found to be nearly coincident with less than 1% variation seen across all bands for all altitudes. While the 'at-sensor' radiance and hence AVRIS DN outputs are observed to change with altitude, both target and background are influenced in the same fashion and hence $TCRs^2$ values and target detection performance remains constant with altitude.

Thus in summary, if the target and background experience the same influences due to altitude, and spatial resolution or sensor noise are not limiting factors, $TCRs^2$ values and detection performance is relatively altitude independent. As the majority of meteorological influences are confined primarily to the 'boundary layer' (less than 2 km altitude) contributions to atmospheric propagation variations from higher altitude sensor deployment is expected to be less significant.

4.7.2 Influence of Time-of-the-day Changes

The approach used in Section 4.7.1 was employed to determine the influence of 'Time-of-the-day' changes on sensor performance. In this case $TCRs^2$ calculations were performed for the 2.5 km altitude nadir looking geometry for the test case of a green camouflage target against eucalypt background. The time of day was varied from 12:00 noon, in 2 hour periods to represent 10:00/14:00, 8:00/16:00 and 6:00/18:00. The solar zenith angle for each of these times is illustrated in Figure 4.7. All other input parameters were held constant.

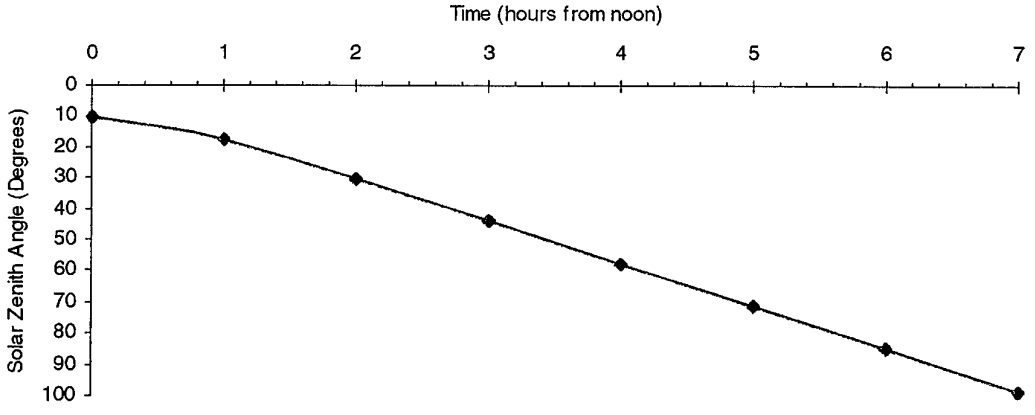

Figure 4.7. Solar zenith angle verses time-of day for Darwin, January 1.

A similar outcome to that seen in Section 4.7.1 was obtained, with the $TCRs^2$ values being nearly identical for all 4 times tested. Again this illustrates if target and background experience the same modulating influence on their signals, and the detection performance is not limited by other factors such as system noise, then the $TCRs^2$ values and detection performance will be 'time-of-day' independent.

Clearly this is not realistic and the AVIRIS sensor's performance will degrade significantly due to intrinsic 'system noise' as the source illumination diminishes early in the morning and late in the evening. This problem is expanded upon, in Section. 4.8

4.8 Sensor Signal to Noise Considerations

All hyperspectral sensor systems have a minimum threshold sensitivity level determined by intrinsic system parameters, including mechanical, optical, and electronic characteristics. To calibrate a sensor system's performance, a noise-equivalent-radiance (*NER*) value can be determined. This *NER* value provides a measure of the actual incoming radiance required generating an output signal equivalent to the system noise. It avoids the otherwise complex and difficult task of measuring the individual noise characteristics of the system. Hence this *NER* value allows for a speedy determination of whether target detection will be limited by system noise or from other sources.

NER calibration data was available for the AVIRIS sensor. Employing this calibration data signal-to-noise ratio (*SNR*) values for a target and background example can be readily determined. This can be achieved by dividing the incoming spectral radiance difference between a given target and background by the appropriate bands *NER*, as outlined by equation 3.3 Section 3. Ideally for accuracy, a statistical approach should be used that includes all samples in given target and background populations.

The green camouflage target and eucalypt background example was used to demonstrate the effects of system noise on detection performance. As only a 'first-cut' indicative guide of the effects of system noise on performance was required, rigorous statistical analysis was not performed. This 'first-cut' approach employed AVIRIS DN sample means for both the target and background. Equation 3.3 was applied to these means to provide a *SNR* value for the absolute difference between the target and background.

As system noise is more likely to influence performance when the source illumination is reduced, predictions were performed for several alternate times of the day. Results for the 'pure-pixel' 2.5 km nadir looking case are presented in Figure 4.8. For more complex scenarios, where target and background separation is likely to be reduced, this 'first-cut' approach may not be of satisfactory accuracy.

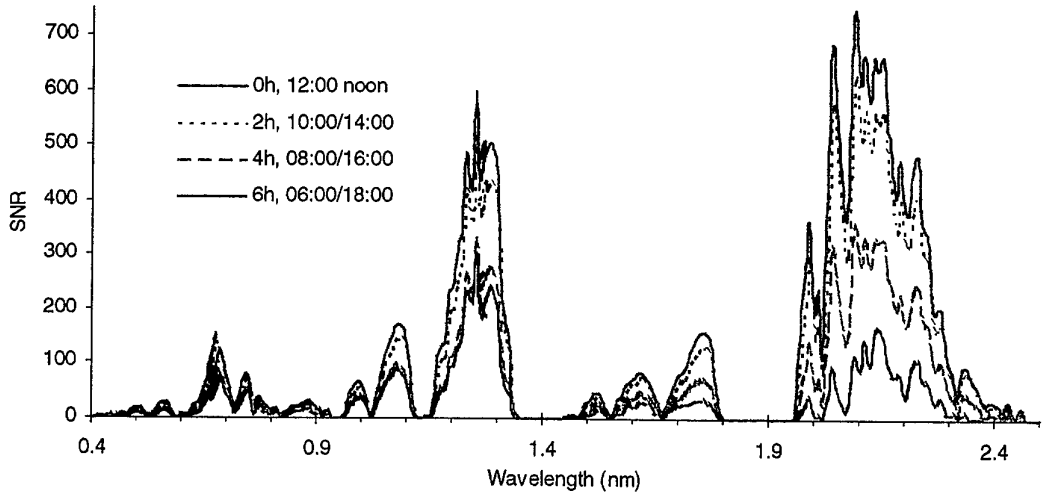

Figure 4.8. Predicted AVIRIS SNR *for a green camouflage target against eucalypt background for various times of the day*

From this data the *SNR* performance for AVIRIS bands 4, 34, 104 and 184 can be determined as illustrated in Table 4.5.

Table 4.5. SNR *verses Time of the Day for AVIRIS Bands 4, 34, 104 and 184*

AVIRIS Band Number	Band Centre (μm)	Predicted *SNR* at 12:00 noon	Predicted *SNR* at 10:00/14:00	Predicted *SNR* at 8:00/16:00	Predicted *SNR* at 6:00/18:00
Band 4	0.399	0.45:1	0.040:1	0.030:1	0.028:1
Band 34	0.673	96:1	84:1	59:1	50:1
Band 104	1.324	146:1	116:1	55:1	44:1
Band 184	2.109	665:1	565:1	333:1	143:1

These results indicate spectral information in Band 4 is dominated by system noise. Band 4 is concluded as not being useable for target detection purposes. This impacts on the 2-band analysis results presented in Section 4.5. Thus the performance enhancement proposed for the Band 4/34 analysis cannot be achieved due to hardware limitations. Thus this 2-band analysis example must be treated as a demonstration only.

Band 184 has *SNR* values in excess of 100:1 for all cases presented. With such large values it is reasonable to conclude that detection performance is not 'system limited' in this band. Bands 34 and 104 demonstrate *SNR* values of sufficient magnitude for the mid-day case (96:1 and 146:1 respectively), but the *SNR* reductions predicted for the early morning/late evening examples, indicate that system noise begins to make appreciable contributions 4 to 6 hours from noon.

In conclusion these results, as expected, illustrate the optimal time for sensor deployment is a window of 2 to 3 hours either side of 12:00 noon although with careful band selection this operational window can be expanded to include morning/evening operation.

An unexpected but important outcome from this *SNR* analysis is the influence of the atmosphere at different times of the day. A significant change in the spectral content of the AVIRIS DN signal (and hence reflected radiation) is observed. A simple percentage reduction change from 12:00 noon was determined to assess this variation. This change is illustrated in Figure 4.9.

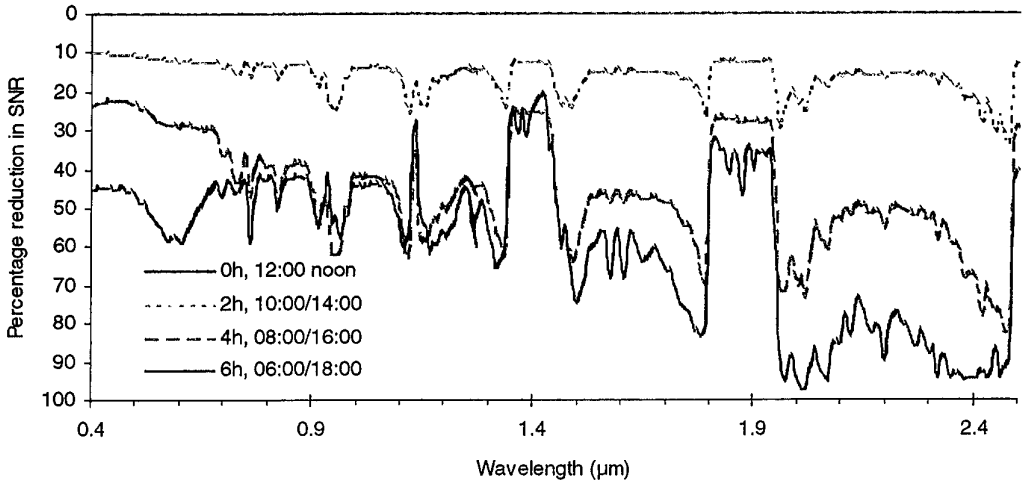

Figure 4.9. AVIRIS DN percentage reduction from 12:00 noon for selected times of the day

A hyperspectral sensor operating in the early morning/late evening (besides being system noise limited) displays a significant spectral bias compared to the midday conditions. At 12 noon the solar zenith angle in the test case is 10.7 degrees while at 6:00/18:00 this angle increases to 85 degrees. The greater zenith angle affords a significantly longer propagation path to the illumination source, and hence spectrally dependent atmospheric propagation losses are more significant.

The two primary loss processes influencing these results are Rayleigh scattering [12] and molecular absorption. 'Large particle' Mie type aerosol scattering is a more broadband process and not expected to give rise to the spectrally dependent changes seen here [15]. The differences seen at the blue end of the spectral range (*ca.* > 0.6 μm) arise from Rayleigh scattering losses. This scattering is proportional to the inverse fourth power of the wavelength and doesn't have significant influence at wavelengths much longer than 0.6 μm. The reduction in signal seen at wavelengths longer than 1.5 μm is caused by increased water vapour absorption. As a tropical,

high humidity constituent profile was used in this modelling the influence of this effect was enhanced.

Thus, in summary, when operating around 12:00 noon, noise appears to be a performance limiting problem only when target and background separation is small, thus the $TCRs^2$ value can provide a useful guide to these limits. When the illumination is reduced 'system noise' becomes considerably more important when determining detection performance. The $TCRs^2$ measure will not be a useful guide on these performance limits (as outlined in Section 4.7.2). Spectrally dependent atmospheric propagation effects must be considered as they can provide a significant bias on target detection results.

5. Conclusions

This report has addressed a wide variety of issues, which are expected to influence the performance of hyperspectral sensors as surveillance tools. Fundamental phenomenology issues have been considered and analysis and results built upon this foundation. The breadth of this study has ranged from investigation into the reflectance properties of materials, the influence of the atmosphere, and modelling a sensor's performance along with data analysis and target detection assessment. Although the initial results are encouraging, they need to be taken as only indicative, due to the limited scope of the analysis.

This study has demonstrated that a sensor operating at hyperspectral resolution has potential in detecting targets such as green camouflage in an eucalypt background with high probability and a low false alarm rate. Such targets would be expected to be difficult to detect by broadband or multi-spectral sensors of similar spatial resolution.

The ability to detect 'sub-pixel' targets is confirmed, with the case presented indicating high detection probabilities and low false alarm rates even when the target occupies only 20% of the pixel. These results are consistent with the finding reported by several other researchers [28,29].

When both targets and background are modified by the same factors, the $TCRs^2$ measure separation remains constant. This conclusion excludes other performance limiting factors such as system noise, the atmospheric propagation and altitude and geometry variations that have the potential to markedly alter the test case's target and background separation and hence detection performance.

Under normal midday operational conditions target detection performance was not system noise limited. Only under low light or poor target and background separation conditions was system noise, as evidenced by a decreased SNR, observed to reduce detection performance appreciably.

A sound procedure has been developed upon which this work can be extended. Key areas of investigation for subsequent studies have been flagged and an approach outlined for the development of target and background data bases and the provision of recommendations relating to the most appropriate spectral channels, their band width and sampling intervals.

5.1 Future work

Complementary work to the above displayed efforts should include a comparison with alternate multispectral and broadband imaging technology. This is important to allow assessment of the benefits of EO technology operating at hyperspectral resolution.

Investigation into the relationship between band-pass and detection performance, with the view of optimisation of a system's performance is also recommended. This approach is expected to provide insight into the best configurations for and limitations of hyperspectral sensors.

Ideally the results and procedures presented could be used to develop a 'training package' to allow assessment and provide recommendations and solutions about the most effective hyperspectral system for a given surveillance scenario.

The requirement of experimentally based validation for this modelling approach is important. This is needed to provide credibility to the results and conclusions made.

6. Acknowledgment

The authors wish to thank Dr. Garry Newsam and Dr. Robert Caprari for their useful discussions and input into the target detection methodology presented in this report.

7. Bibliography

1. Anderson, R., Malila, W., Maxwell, R. Reed, L., 1994, *Military Utility of Multispectral and Hyperspectral Sensors,* Report No. 246890-3-F, Infrared Information Analysis Centre (IRIA) State of the Art Reports.

2. Barducci, A. Pippi, I., 1995, *MIVIS Evaluation for Hyperspectral Sensing of the Environment in Remote Sensing for Agriculture, Foresty and Natural Resources, SPIE* , 2585, 241-246.

3. Shen, S.S., 1996, *Relative Utility of HYDICE and Mutispectral Data for Object Detection, Identification and Abundance Estimation in Hyperspectral Remote Sensing and Application Performance, SPIE,* 2821, 256-267.

4. DePersia, A.T., Bowman, A.P., Giles, A.L., Winter, E.M., Badik, F., Schlangen, M., Lucy, P., Williams, T., Johnson, J., Hinrichs, J., Horton, K., Allen, G., Stocker, A. Oshagan, A. Schaff, B., Kendall, B., Carter, M.R., Bennett, C.L., Fields, D.J., 1995, *ARPA'S Hyperspectral Mine Detection Program, Conference Proceedings of the International Symposium on Spectral Sensing Research,* 26 Nov.-1 Dec. 1995, Melbourne, Australia.

5. Portigal, F.P. Otten, L.J., 1996, *Non-linear unmixing of simulated MightySat FTHSI data for target detection limits in a humid tropical scene in, Algorithms, SPIE,* 2758, 84 -90.

6. Gat, N., Subramanian, S., Barhen, J., Toomarian, N., 1996, *Spectral Imaging Applications: Remote Sensing, Environmental Monitoring, Medicine, Military Operations, Factory Automation and Manufacturing, SPIE,* 2962, 63-77.

7. Bishop, K.D. Diestel, M.J., 1996,*The Airborne Remote Earth Sensing (ARES) Program: An Operational Airborne MWIR Imaging Spectrometer and Applications, SPIE,* 2821, 183-194.

8. Babey, S.K. Anger, C.D., 1995, *Potential for the application of airborne hyperspectral remote sensing techniques to industrial inspection, SPIE,* 2599, 302-307.

9. Vane, G. O'Green, R. Chrien, T.G. Enmark, H.T. Hansen, E.G. Porter, W.M., 1993, *The Airborne Visible/Infrared Imaging Spectrometer (AVIRIS), Remote Sens. Environ.,* 44, 127-143.

10. Sliney, A., Wolbarsht, M., 1980, *Saftey with Lasers and Other Optical Sources,* Plenum Press, New York/London.

11. Banwell, C.N., 1972, *Fundamental of Molecular Spectroscopy* 2nd *Edition,* McGraw-Hill Book Company (UK) Limited, London.

12. Asrar, G. Ed., 1989, *Theory and Applications of Optical Remote Sensing,* John Wiley and Sons, New York.

13. Satterwhite, M.B. Ponder Henley, J., 1990, *Hyperspectral Signatures (400 to 2500nm) of Vegetation, Minerals, Soils, Rocks, and Cultural Features: Laboratory and Field Measurements,* Report ETL-0573, US Army Engineer Topographic Laboratories, Fort Belvoir, Virginia.

14. *The Nonconventional Exploitation Factors (NEF) Modelling Spectral Catalogue Ver 4.0,* 1992, ORD 311-92.

15. Berk, A Bernstein, L.S. Robertson, D.C., 1989, *MODTRAN : A Moderate Resolution Model for Lowtran7*, GL-TR-89-0122, Geophysics Laboratory, United States Air Force Systems Command, Hanscom Air Force Base, Massachusetts.

16. Anderson, G.P. Kneizys, F.X. Chetwynd, J.H. Wang, J. Hoke, M.L. Rothman, L.S. Kimball, L.M. Mclatchey, R.A., Shettle, E.P., Clough, S.A., Gallery, W.O., Abreu, L. W., Selby, J.E.A., 1995, *FASCODE/MODTRAN/LOWTRAN: Past/Present/Future, 18th Annual Review Conference on Atmospheric Transmission Models*, Hanscom Air Force Base, Massachusetts, 6-8 June 1995

17. Kneizys, F.X. Shettle, E.P. Abreu, L.W. Anderson, G.P. Chetwynd, J.H. Jr., Gallery, W.O. Selby, J.E.A. Clough, S.A., 1988, *Users Guide to LOWTRAN7*, AFGL-TR-88-0177, Air Force Geophysics Laboratory, Hanscom Air Force Base, Massachusetts.

18. Wang, J. Anderson, G.P., 1994, *Validation of FASCOD3 and MODTRAN3: Comparison of model calculations with Interferometer Observations from SPECTRE and ITRA*, SPIE, 2309, 220-231.

19. Anderson, G.P., Chetwynd, J.H., 1992, *FASCOD3 Preliminary Version: FASCOD3P*, Hanscom Air Force Base, Massachusetts.

20. Curtiss, B. Goetz, A.F.H., 1994, *Field Spectrometry, Techniques and Instrumentation, International Symposium on Spectral Sensing Research.*

21. Westmoreland, S. Mertz, F.C., 1998, *Private communication*, Photon Research Associates, Inc. USA.

22. Cornette, W.M. Westmoreland, S.J., 1998, *Mosart-Modtran difference budget, 21st Annual Review Conference on Atmospheric Transmission and Radiance Models*, Hanscom Air Force Base, Massachusetts, 9-11 June 1998.

23. Cornette, W.M., 2000, *Private commumication*, NIMA, USA.

24. Fukunaga, K., 1990, *Introduction to Statistical Pattern Recognition, 2nd Edition*, Academic Press, Inc., Boston.

25. Koch, G.S. Jr., Link, R.F., 1971, *Statistical Analysis of Geological Data*, Dover Publications, Inc., New York.

26. Manly, B. F. J., 1994, *Multivariate Statistical Methods - A Primer, 2nd Edition*, Chapman and Hall, London.

27. Jain, A.K., Chandrasekaran, B., 1982, *Handbook of Statistics, Dimensionality and Sample Size Considerations in Pattern Recognition Practice*, Volume 2, North-Holland Publishing Company.

28 Shettigara, V.K., Kempinger, S.G., Nitschke, P.E., 2000, *Surveillance Capabilities of Compact Airborne Spectrographic Imager and Hyperspectral Mapper Sensors*, DSTO-TR-0897.

29 Cross, A.M., Settle, J.J., Drake, N.A., Paivinen, R.T.M., 1991, Subpixel measurement of tropical forest cover using AVHRR data, Int. J. Remote Sensing, 12, 1119-1129.

Appendix A

Reflectance Files as Collected from ASD Spectrometer and Used for all Subsequent Analysis.

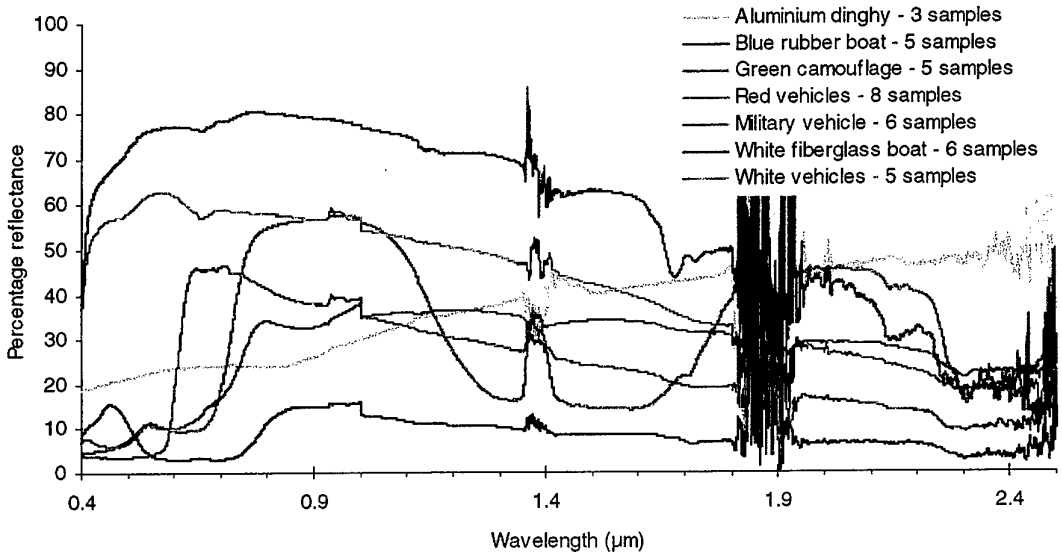

Figure A.1. Target mean reflectance collected by the ASD spectrometer

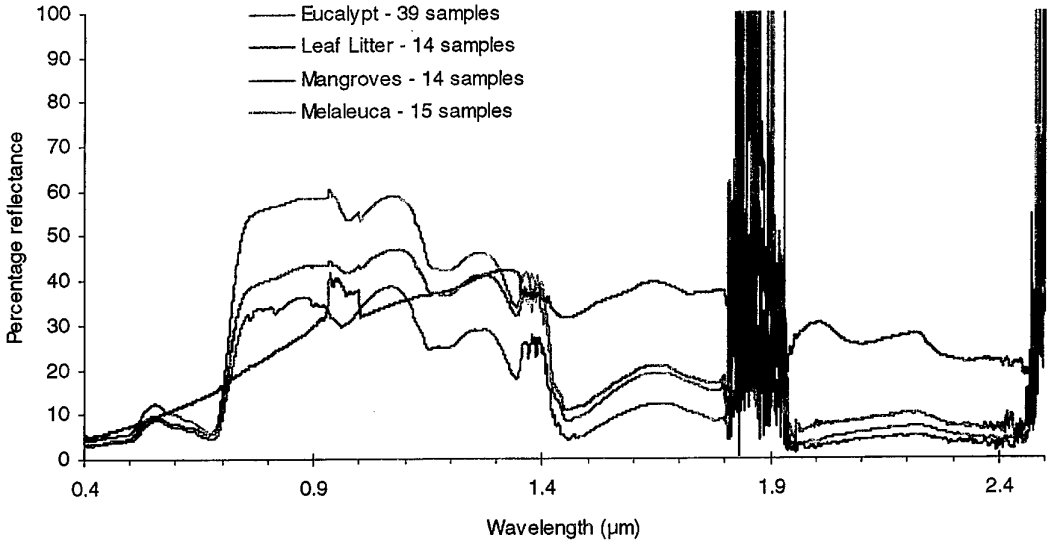

Figure A.2. Background mean reflectance collected by the ASD spectrometer.

Appendix B

Digital Number (DN) Values Generated from the Corresponding Reflectance Files in Appendix A

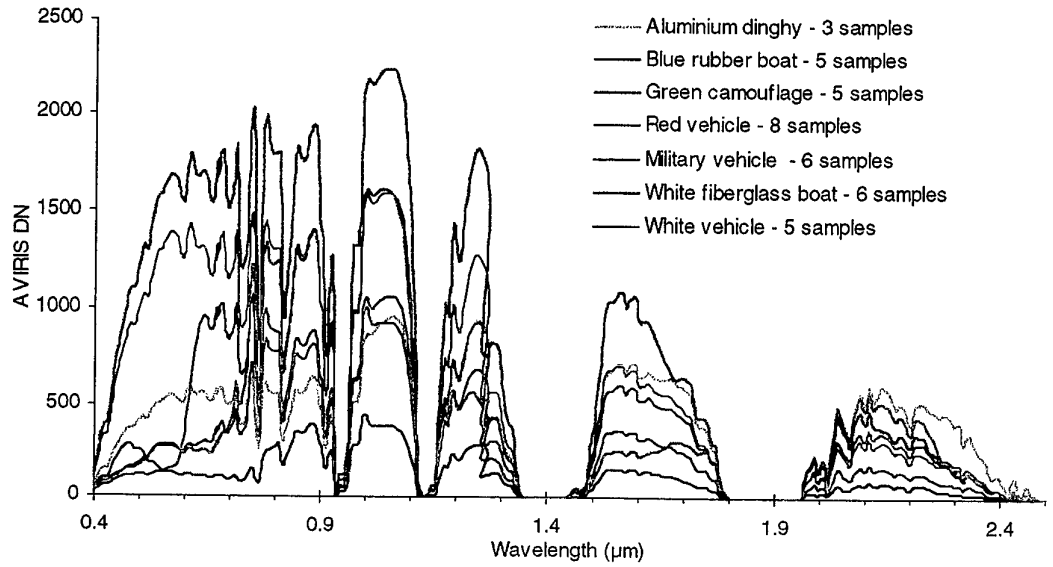

Figure B.1. Predicted mean AVIRIS DN values for targets used in the report

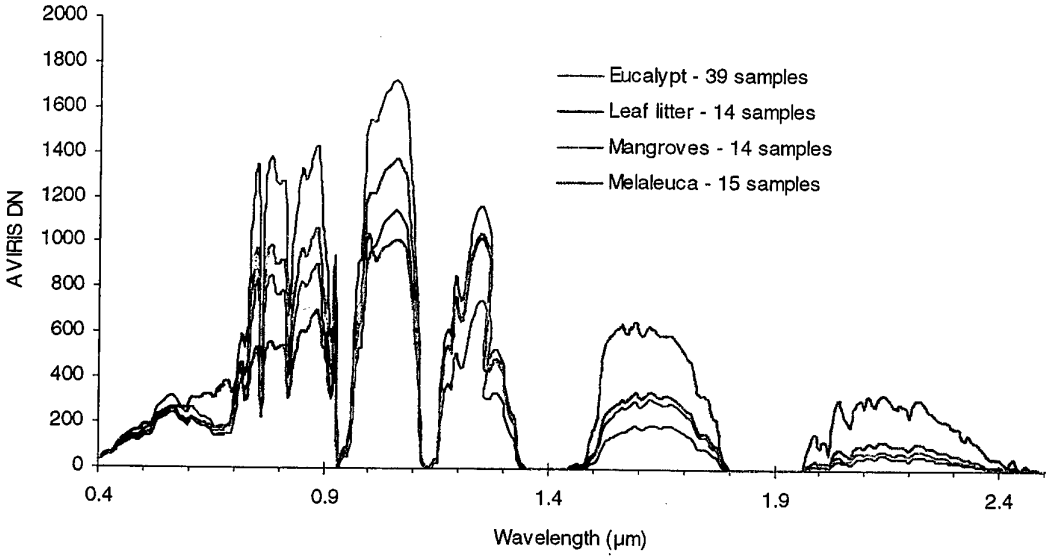

Figure B.2. Predicted mean AVIRIS DN values for backgrounds used in the report

Appendix C

TCRs² Separation of Selected Target and Background Populations.

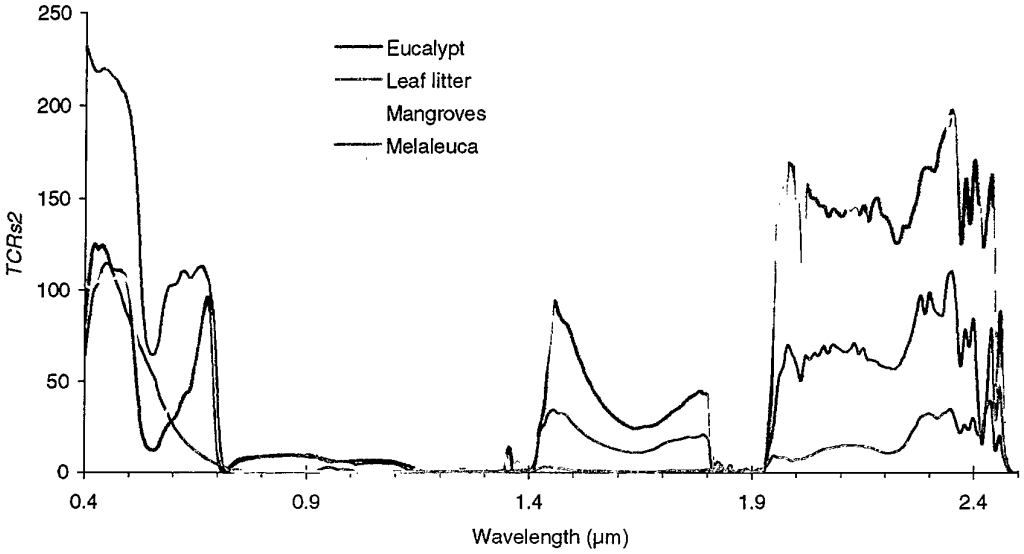

Figure C.1. TCRs² separation of an aluminium dinghy against background

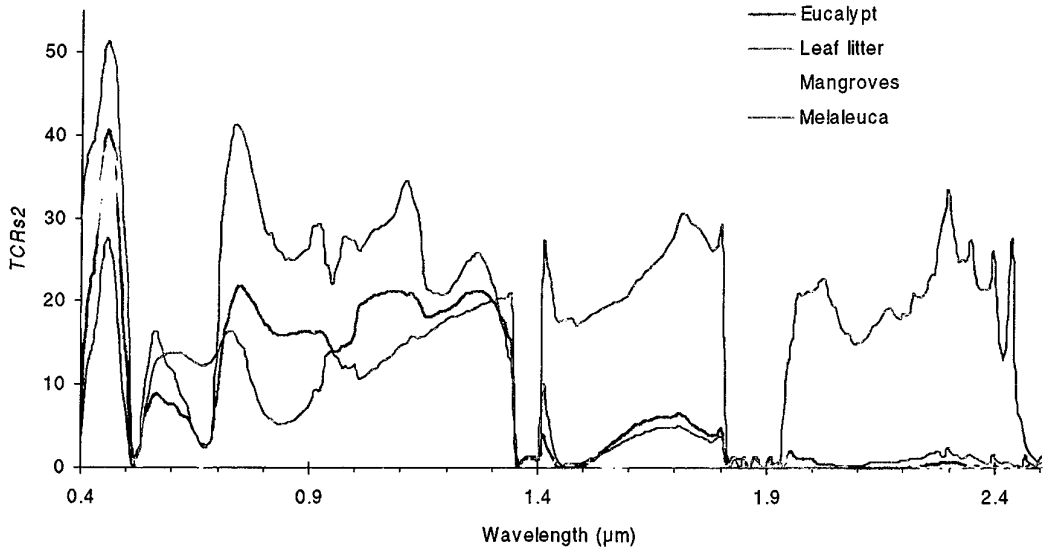

Figure C.2. TCRs² separation of a blue rubber boat against background

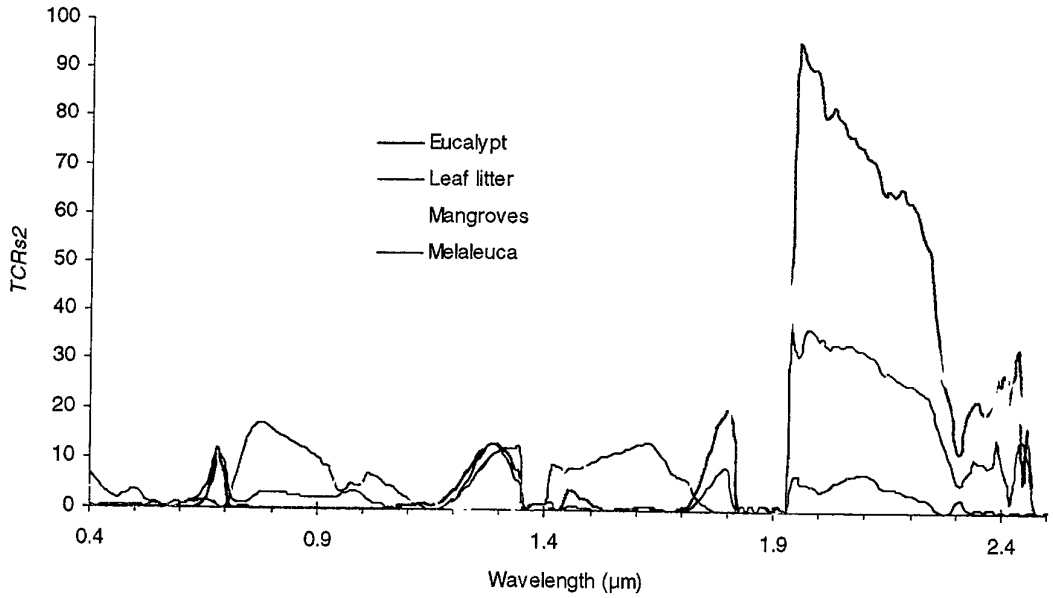

Figure C.3. TCRs² separation of green camouflage against background

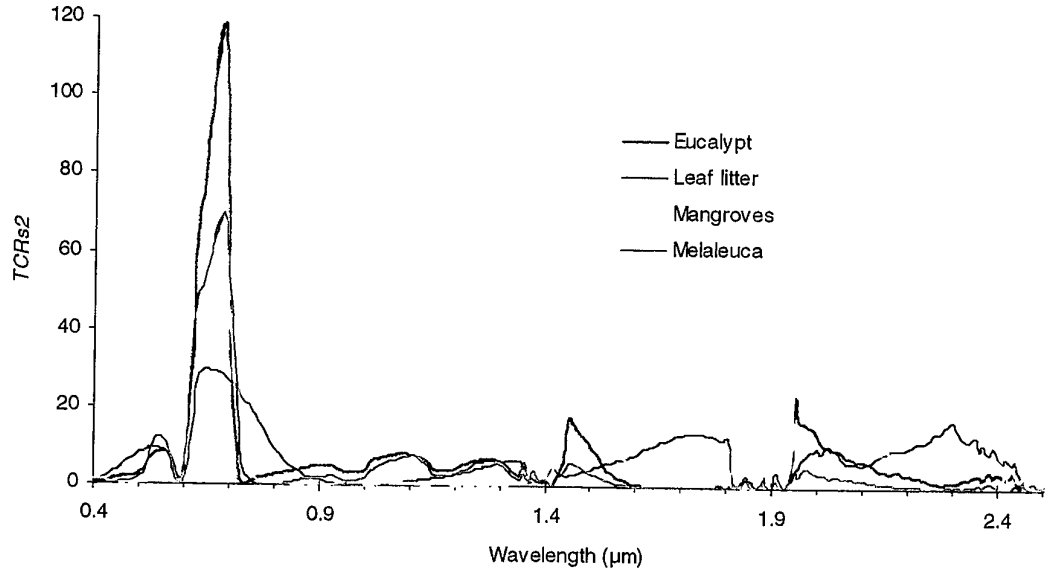

Figure C.4. TCRs² separation of a red vehicle against background red vehicle

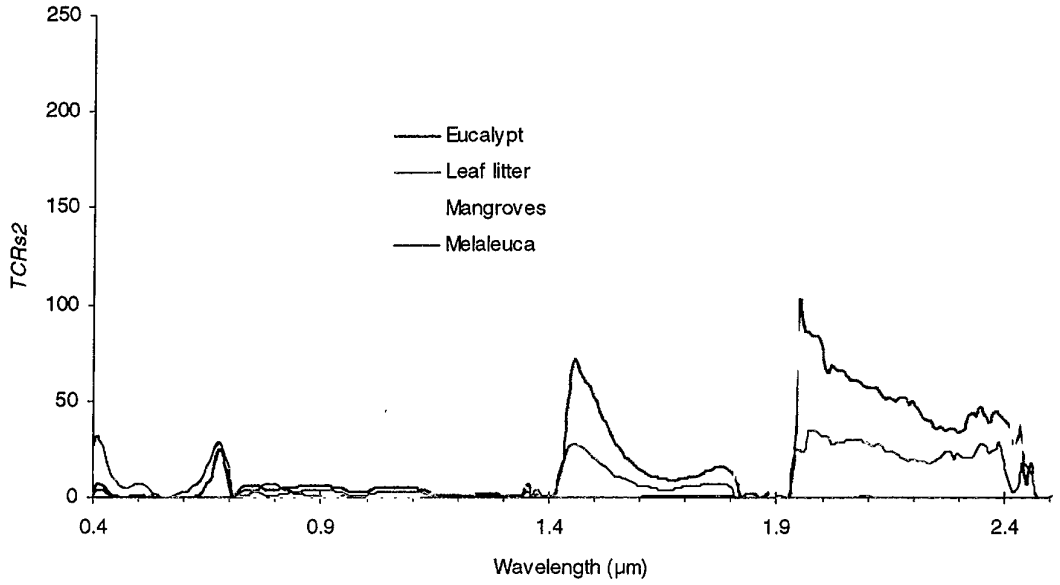

Figure C.5. TCRs² separation of a military vehicle against background

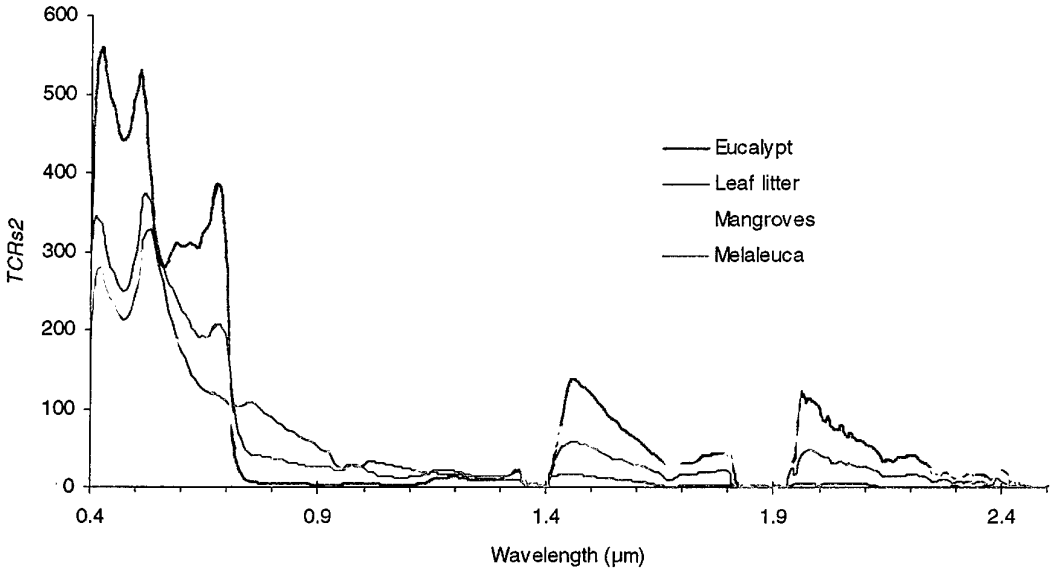

Figure C.6. TCRs² separation of a white fibreglass boat against background

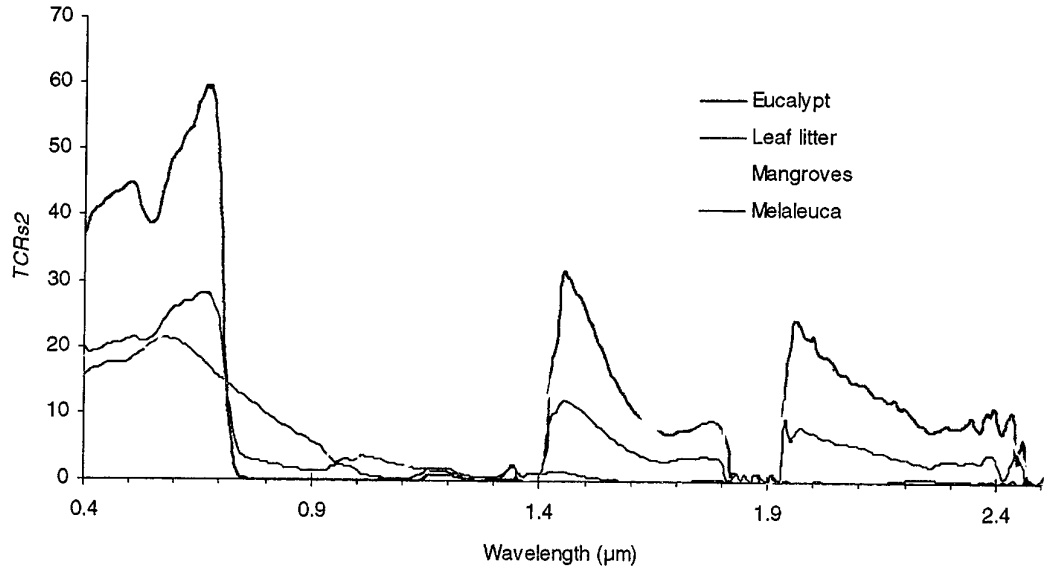

Figure C.7. TCRs² separation of a white vehicle against background

Appendix D

Minimum $TCRs^2$ Separation between Targets and All Backgrounds.

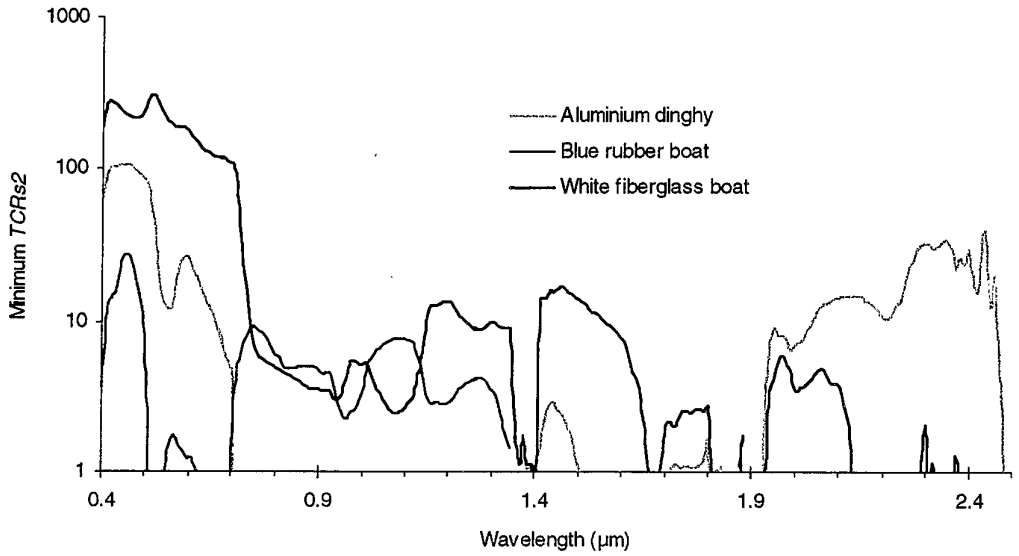

Figure D.1. Minimum separation between littoral targets and all backgrounds.

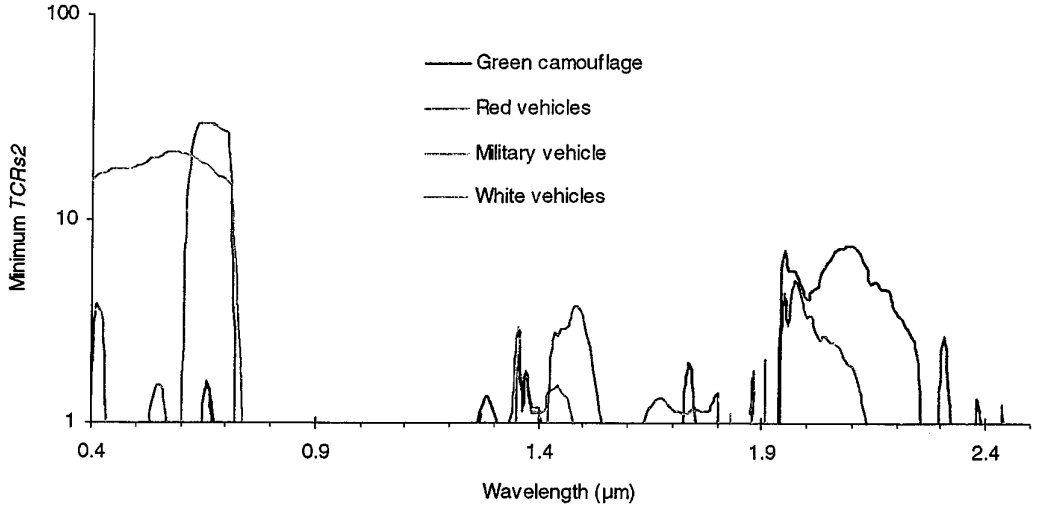

Figure D.2. Minimum separation between terrestrial targets and all backgrounds.

Appendix E

Sample Distributions of a Green Camouflage Target and an Eucalypt Background.

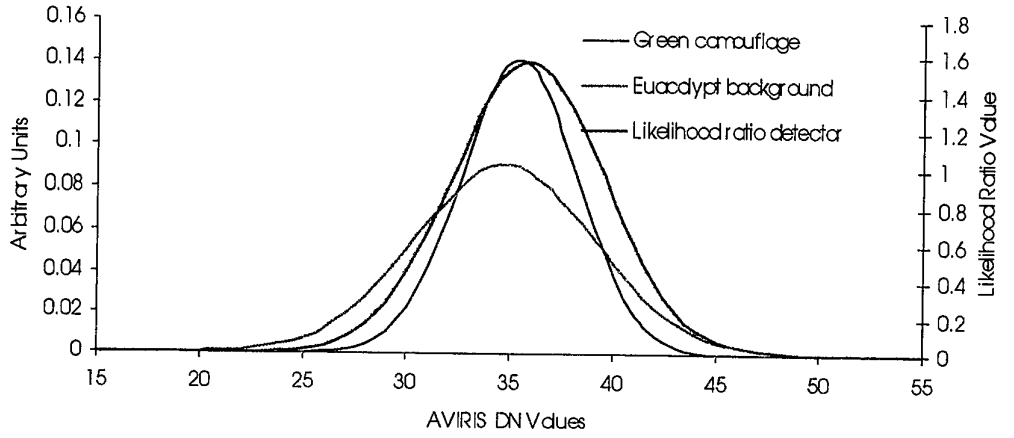

Figure E.1. AVIRIS Band 4, likelihood ratio detector analysis for a green camouflage target and euacalypt background.

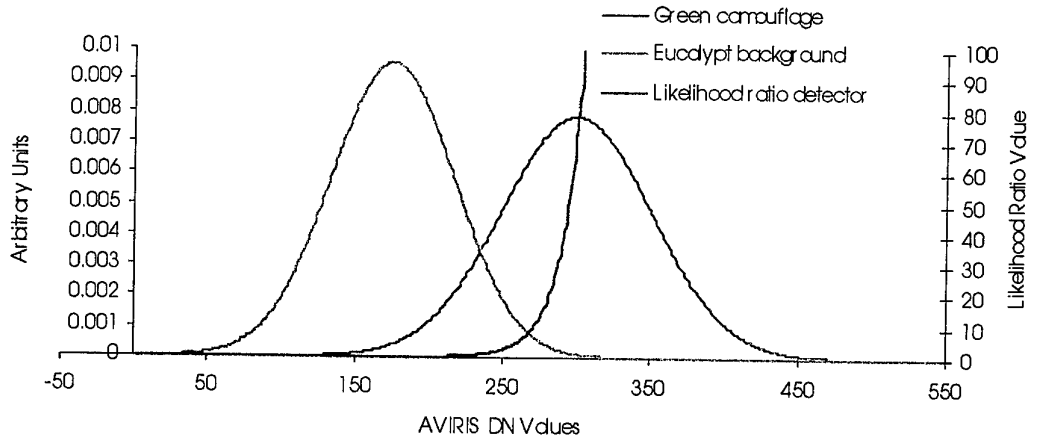

Figure E.2. AVIRIS Band 34, likelihood ratio detector analysis for a green camouflage target and euacalypt background.

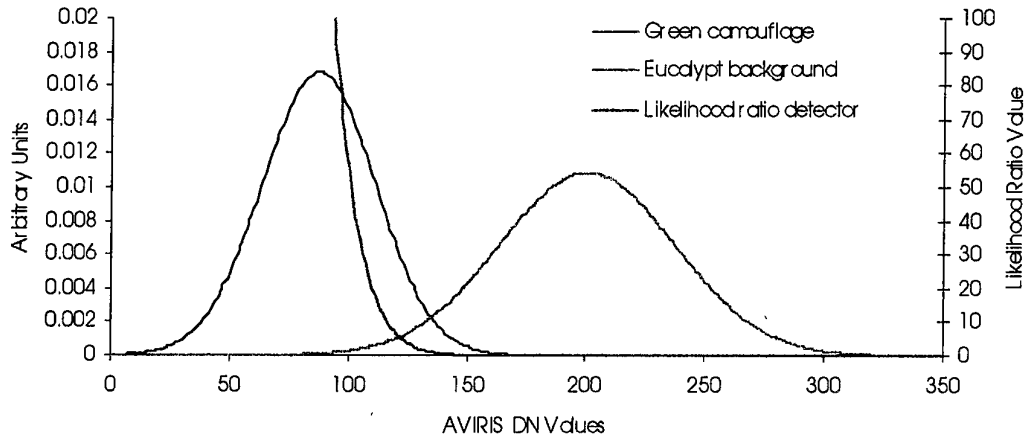

Figure E.3. AVIRIS Band 104, likelihood ratio detector analysis for a green camouflage target and euacalypt background.

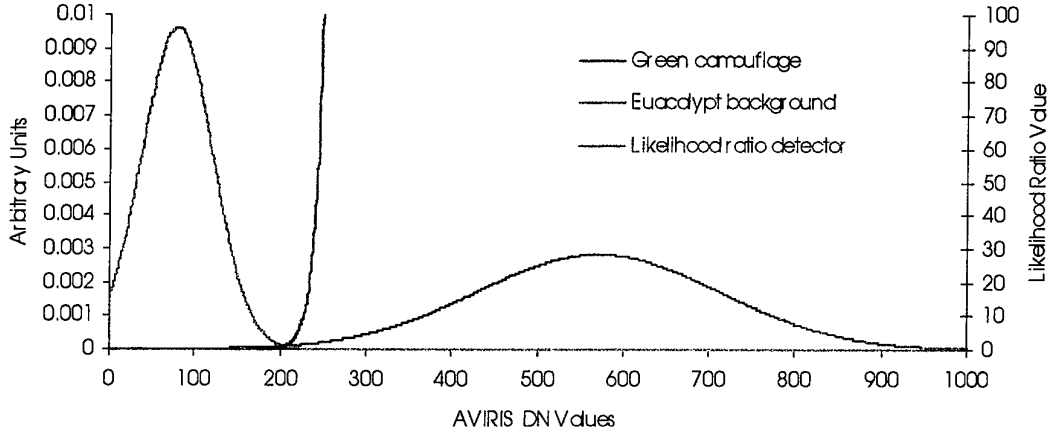

Figure E.4. AVIRIS Band 184, likelihood ratio detector analysis for a green camouflage target and euacalypt background.

DISTRIBUTION LIST

An Investigation of Target Detection Ability Using Spectral Signatures at Hyperspectral Resolution.

T. P. Bubner, S. K. Kempinger and V. K. Shettigara.

AUSTRALIA

DEFENCE ORGANISATION

Task Sponsor		1
S&T Program		
Chief Defence Scientist FAS Science Policy AS Science Corporate Management	shared copy	1
Director General Science Policy Development		1
Counsellor Defence Science, London		Doc Data Sheet
Counsellor Defence Science, Washington		Doc Data Sheet
Counsellor Defence Science, Thailand		Doc Data Sheet
Scientific Adviser Policy and Command		1
Navy Scientific Adviser		Doc Data Sheet and Distribution List
Scientific Adviser - Army		Doc Data Sheet and Distribution List
Air Force Scientific Adviser		1
Director Trials		1
Aeronautical and Maritime Research Laboratory		
Director		1
Electronics and Surveillance Research Laboratory		
Director		Doc Data Sheet
Chief of Surveillance Systems Division		1
Research Leader, Imagery Systems, SSD		1
Research Leader, Maritime Systems, SSD		1
Head, Imaging Electro Optical Systems, SSD		1
Head, Image Analysis and Exploitation, SSD		1
Head, Imaging Radar Systems, SSD		1
Task Manager: V Shettigara		1
Author(s): T Bubner		2
S Kempinger		2
V Shettigara		2
G Bain, AED		1
E Hunt, SSD		1
G Fowler, SSD		1
S Angeli, SSD		1
R Caprari, SSD		1
P Johnson, SSD		1

DSTO Library	
Library Fishermans Bend	1
Library Maribyrnong	1
Library Salisbury	2
Australian Archives	1
Library, MOD, Pyrmont	Doc Data Sheet
Library, MOD, HMAS Stirling	Doc Data Sheet
Document Exchange	
US Defense Technical Information Center	2
UK Defence Research Information Centre	2
Canada Defence Scientific Information Service	1
NZ Defence Information Centre	1
Capability Systems Staff	
Director General Maritime Development (Doc Data Sheet only)	
Director General Aerospace Development	1
Knowledge Staff	
Director General Command, Control, Communications and Computers (DGC4) (Doc Data Sheet only)	
Director General Intelligence, Surveillance, Reconnaissance, and Electronic Warfare (DGISREW)R1-3-A142 CANBERRA ACT 2600	Doc Data Sheet
Director General Defence Knowledge Improvement Team (DGDKNIT) R1-5-A165, CANBERRA ACT 2600	Doc Data Sheet
Intelligence Program	
HAEG, DIGO	1
D Carmody, DIGO	1
T O'Leary, DIGO	1
DGSTA Defence Intelligence Organisation	1
Manager, Information Centre, Defence Intelligence Organisation	1
C4ISREW	
DOISD	1
Corporate Support Program	
OIC TRS, Defence Regional Library, Canberra	1
SPARES	
DSTO Salisbury Research Library	5
Total number of copies:	50

DEFENCE SCIENCE AND TECHNOLOGY ORGANISATION DOCUMENT CONTROL DATA	1. PRIVACY MARKING/CAVEAT (OF DOCUMENT)

2. TITLE	3. SECURITY CLASSIFICATION (FOR UNCLASSIFIED REPORTS THAT ARE LIMITED RELEASE USE (L) NEXT TO DOCUMENT CLASSIFICATION)
An Investigation of Target Detection Ability Using Spectral Signatures at Hyperspectral Resolution.	Document (U) Title (U) Abstract (U)

4. AUTHOR(S)	5. CORPORATE AUTHOR
T. P. Bubner, S. K. Kempinger and V. K. Shettigara.	Electronics and Surveillance Research Laboratory PO Box 1500 Salisbury SA 5108 Australia

6a. DSTO NUMBER	6b. AR NUMBER	6c. TYPE OF REPORT	7. DOCUMENT DATE
DSTO-TR-0807	AR-010-899	Technical Report	February 2001

8. FILE NUMBER	9. TASK NUMBER	10. TASK SPONSOR	11. NO. OF PAGES	12. NO. OF REFERENCES
9505/017/0073/01(U)	JNT 96/306	DASD	47	29

13. URL on the Worldwide Web	14. RELEASE AUTHORITY
http://www.dsto.defence.gov.au/corporate/reports/DSTO-TR-0807.pdf	Chief, Surveillance Systems Division

15. SECONDARY RELEASE STATEMENT OF THIS DOCUMENT

Approved for public release

OVERSEAS ENQUIRIES OUTSIDE STATED LIMITATIONS SHOULD BE REFERRED THROUGH DOCUMENT EXCHANGE, PO BOX 1500, SALISBURY, SA 5108

16. DELIBERATE ANNOUNCEMENT

No Limitations

17. CASUAL ANNOUNCEMENT Yes

18. DEFTEST DESCRIPTORS

Target acquisition, Spectrum signatures, Performance evaluation

19. ABSTRACT

This report addresses a variety of issues expected to influence the performance of airborne high spectral resolution (hyperspectral) Electro-Optic (EO) sensors when used as surveillance tools. Fundamental phenomenology issues have been considered with the breadth of this study ranging from investigation into the reflectance properties of materials, the influence of the atmosphere, and modelling of a sensor's performance. Simple data analysis and target detection assessment techniques including Target to Clutter Ratio measures and single and multiple band 'likelihood ratio detection' have been employed on an illustrative example. Initial results are promising, indicating high probabilities of detection with low false alarm rates for the test example.